A&A 556, A120 (2013)
DOI: 10.1051/0004-6361/201322026

Astronomy & Astrophysics

Unveiling the nature of INTEGRAL objects through optical spectroscopy⋆

X. A new multi-year, multi-observatory campaign

N. Masetti[1], P. Parisi[2], E. Palazzi[1], E. Jiménez-Bailón[3], V. Chavushyan[4], V. McBride[5,6], A. F. Rojas[7], L. Steward[5,6], L. Bassani[1], A. Bazzano[2], A. J. Bird[8], P. A. Charles[8], G. Galaz[7], R. Landi[1], A. Malizia[1], E. Mason[9], D. Minniti[7,10], L. Morelli[11,12], F. Schiavone[1], J. B. Stephen[1], and P. Ubertini[2]

[1] INAF – Istituto di Astrofisica Spaziale e Fisica Cosmica di Bologna, via Gobetti 101, 40129 Bologna, Italy
e-mail: masetti@iasfbo.inaf.it
[2] INAF – Istituto di Astrofisica e Planetologia Spaziali, via Fosso del Cavaliere 100, 00133 Rome, Italy
[3] Instituto de Astronomía, Universidad Nacional Autónoma de México, Apartado Postal 70-264, 04510 México D.F., México
[4] Instituto Nacional de Astrofísica, Óptica y Electrónica, Apartado Postal 51-216, 72000 Puebla, México
[5] South African Astronomical Observatory, PO Box 9, Observatory 7935 Cape, South Africa
[6] Department of Astronomy, University of Cape Town, Private Bag X3, Rondebosch 7701 Cape Town, Republic of South Africa
[7] Departamento de Astronomía y Astrofísica, Pontificia Universidad Católica de Chile, Casilla 306, 22 Santiago, Chile
[8] School of Physics & Astronomy, University of Southampton, Highfield, SO17 1BJ Southampton, UK
[9] Space Telescope Science Institute, 3700 San Martin Drive, Baltimore, MD 21218, USA
[10] Specola Vaticana, 00120 Città del Vaticano
[11] Dipartimento di Fisica ed Astronomia "G. Galilei", Università di Padova, vicolo dell'Osservatorio 3, 35122 Padova, Italy
[12] INAF-Osservatorio Astronomico di Padova, Vicolo dell'Osservatorio 5, 35122 Padua, Italy

Received 6 June 2013 / Accepted 20 June 2013

ABSTRACT

Within the framework of our program (running since 2004) of identification of hard X-ray INTEGRAL sources through optical spectroscopy, we present the results concerning the nature of 33 high-energy objects. The data were acquired with the use of six telescopes of different sizes and from one on-line archive. The results indicate that the majority of these objects (23 out of 33) are active galactic nuclei (AGNs), whereas 10 are sources in the local Universe with eight of which in the Galaxy and two in the Small Magellanic Cloud (SMC). Among the identified AGNs, 13 are of Type 1 (i.e., with broad emission lines), eight are of Type 2 (with narrow emissions only), and two are X-ray bright, optically normal galaxies with no apparent nuclear activity in the optical. Six of these AGNs lie at high redshift ($z > 0.5$). Concerning local objects, we found that five of them are Galactic cataclysmic variables, three are high-mass X-ray binaries (two of which lying in the SMC), one is a low-mass X-ray binary, and one is classified as a flare star that is likely of RS CVn type. The main optical properties and inferred physical characteristics of these sources are presented and discussed.

Key words. galaxies: Seyfert – quasars: emission lines – X-rays: binaries – novae, cataclysmic variables – stars: flare

1. Introduction

One principal objective of the INTEGRAL mission (Winkler et al. 2003) is the systematic survey of the whole sky in the hard X-ray band above 20 keV. This is made possible thanks to the unique imaging capability of the IBIS instrument (Ubertini et al. 2003) in this spectral range, which allows the detection of sources at the mCrab[1] level with a typical localization accuracy of a few arcmin. The fourth and latest IBIS catalogue (Bird et al. 2010) contains more than 700 hard X-ray sources detected in the 20–100 keV band down to an average flux level of about 1 mCrab with a positional accuracy that is better than ∼5 arcmin. Similarly, the 17–60 keV surveys published by Krivonos et al. (2010, 2012) contain about 500 and 400 sources, respectively (partly overlapping between them and with the catalogue of Bird et al. 2010), with sensitivity and localization precision comparable to that of Bird et al. (2010).

A non-negligible fraction (for instance, ∼30% in the case of the survey of Bird et al. 2010) of these objects had no obvious counterpart at other wavelengths and therefore could not be associated with any known class of high-energy emitting objects. Multiwavelength observational campaigns on these unidentified sources are therefore mandatory to pinpoint their nature.

Several approaches using X-ray data analysis have shown their effectiveness in identifying the nature of some of these new INTEGRAL sources, such as X-ray timing (e.g., Walter et al. 2006; Sguera et al. 2007; Del Santo et al. 2007; La Parola et al. 2010) or spectroscopy and imaging (see for instance Rodriguez et al. 2010; Malizia et al. 2010; Tomsick et al. 2012, and references therein).

⋆ Based on observations collected at the following observatories: Cerro Tololo Interamerican Observatory (Chile); Observatorio del Roque de los Muchachos of the Instituto de Astrofísica de Canarias (Canary Islands, Spain); Astronomical Observatory of Bologna in Loiano (Italy); Astronomical Observatory of Asiago (Italy); Observatorio Astronómico Nacional (San Pedro Mártir, Mexico); South African Astronomical Observatory (Sutherland, South Africa); and Australian Astronomical Observatory (Siding Spring, Australia).

[1] 1 mCrab ≅ 2×10^{-11} erg cm^{-2} s^{-1} with a slight dependence on the reference energy range.

Alternatively and also effectively, cross-correlation with soft X-ray catalogues and consequent optical spectroscopy on thereby selected candidates allows the determination of the nature and the main multiwavelength characteristics of unidentified or poorly studied hard X-ray objects. This is especially important, given that very interesting classes of objects can be found among hard X-ray emitting sources due to the high power of penetration of this radiation through dust and hydrogen clouds.

For instance, this approach is vital for the search for nearby Compton-thick active galactic nuclei (AGNs) with a line-of-sight hydrogen column $N_{\rm H} > 10^{24}$ cm^{-2}. Because of the strong absorption in their host galaxies, their activity is depressed in the optical waveband; as a consequence, heavily absorbed AGNs and Compton thick objects are often found among the faintest optical counterparts of INTEGRAL sources. Finding even a few of these highly absorbed active galaxies, especially in the local Universe, is of great importance to estimate their fraction among the hard X-ray AGN population (e.g., Malizia et al. 2009).

The same effect is seen in Galactic objects since intrinsic absorption characterizes some of the new types of hard X-ray binaries detected by INTEGRAL (see e.g. Sguera et al. 2006).

All the above means that a fraction of these objects can substantially be absorbed which thus appear relatively faint in the optical. Therefore, follow-up with medium-sized telescopes (of 4 m-class, for instance) is mandatory to properly identify and study the longer-wavelength counterparts of these hard X-ray sources.

The use of this class of telescopes also allows us to study the faint end of the distribution of high-energy, high-z AGNs lying at a mean distance ~5 times larger than that of the average of this type of objects known up to now (see Masetti et al. 2012a). It is even possible that these objects are indeed different from those at lower redshifts in the sense that they belong to a subclass of extreme blazars that emit the bulk of their power in the hard X-ray band (Ghisellini et al. 2011).

Here, we carry on the work of identifying INTEGRAL sources which we started in 2004 and which permitted us to identify more than 170 sources up to now by means of optical spectroscopy (see Masetti et al. 2004, 2006a,b,c,d, 2008a, 2009, 2010, 2012a [hereafter Papers I-IX, respectively], 2007, 2008b; Maiorano et al. 2011). The optical spectra of the firm or likely counterparts of 30 unidentified, unclassified, or poorly studied sources belonging to one or more IBIS surveys (Bird et al. 2010; Coe et al. 2010; Krivonos et al. 2010, 2012; Bottacini et al. 2012; Grebenev et al. 2013) are shown in this paper. We moreover added to our sample the spectra of two INTEGRAL sources reported in Ricci et al. (2012) and one in Townsend et al. (2011), thus reaching a total of 33 objects hereby explored. In this work, we also take the opportunity to correct the redshift of source IGR J16388+3557 reported in Paper IX. Optical spectroscopy for this sample of sources was acquired using six different telescopes and one public spectroscopic archive; among these facilities, the use of medium-sized telescopes allows us to pursue the exploration of the issues outlined above.

The paper is structured as follows. In Sect. 2, we outline the approach we used to choose the sample of INTEGRAL and optical objects considered in this work. In Sect. 3, a description of the observations is given. Section 4 shows and discusses the results with an update of the statistics on the identifications of INTEGRAL sources available until now. Conclusions are reported in Sect. 5.

We recall that the main results presented here and the information concerning the INTEGRAL sources that have been identified up to now (by us or by other groups) using optical or near-infrared (NIR) observations are listed in a web page[2] that we maintain as a service to the scientific community (Masetti & Schiavone 2008). Unless otherwise stated, errors and limits in this paper are reported at 1σ and 3σ confidence levels, respectively. Moreover, this work supersedes the optical results presented in the preliminary analyses of Masetti et al. (2012b) and Parisi et al. (2012).

2. Sample selection

Using the same approach as in our previous Papers I–IX, we considered the IBIS surveys of Bird et al. (2010), Krivonos et al. (2010, 2012), Coe et al. (2010), Grebenev et al. (2013), and the *Swift*/INTEGRAL ("SIX") joint catalogue of Bottacini et al. (2012). Among them, we selected unidentified or unclassified hard X-ray sources containing a single bright soft X-ray object within the IBIS 90% confidence level error box. The latter information was obtained from either the ROSAT all-sky bright source catalogue (Voges et al. 1999), *Swift*/XRT pointings (from Krivonos et al. 2009; Rodriguez et al. 2009; Maiorano et al. 2010; Sturm et al. 2011; Kennea 2011; Malizia et al. 2011; Landi et al. 2012a; Luna et al. 2012; Molina et al. 2012a; Parisi et al. 2012, and from the XRT archive[3]), or *Chandra* observations (Kaur et al. 2010; Tomsick et al. 2008). As stressed and demonstrated (see Stephen et al. 2006 and Papers I-IX), this procedure is extremely effective in substantially reducing the search area and in pinpointing a putative optical counterpart within the corresponding (sub)arcsecond-sized soft X-ray error box.

To increase the positional accuracy of some of the selected sources (especially those lying along the Galactic plane, where the source confusion can be an important issue), we also cross-correlated the above selected sources with radio catalogues, such as the NVSS (Condon et al. 1998), SUMSS (Mauch et al. 2003), and MGPS (Murphy et al. 2007) surveys. This method allowed the further reduction of the soft X-ray position uncertainty down to less than 2″ for a few sources, and hence the possibility of determining the actual counterpart with a higher degree of accuracy.

Among these objects, we then chose those with a single possible optical counterpart with magnitude $R \lesssim 20$ on the DSS-II-Red survey[4], so that optical spectroscopy could be obtained with a reasonable signal-to-noise ratio (S/N) with telescopes having an aperture of at least 1.5 m. This allowed us to select 21 IBIS sources.

In four more cases, two soft X-ray sources were found within the corresponding IBIS error circle (Landi et al. 2012b, 2013; Molina et al. 2012b; Tomsick et al. 2012). In these occurrences, we focused on the optical object associated with the brighter soft X-ray source, but we attempted to get optical spectroscopy on the other putative counterpart as well when feasible.

To this sample, we added the object RX J0101.8−7223 (Townsend et al. 2011 and references therein) and the newly-discovered sources IGR J02045−1156 and IGR J02574−0303 (Ricci et al. 2012) because an arcsecond-sized soft X-ray position and a likely optical counterpart are made available by those authors for them.

We next relaxed the search criterion described at the beginning of this Section by considering the IBIS 99% error circles. This allowed us to select four more cases (indicated in Table 1)

[2] http://www.iasfbo.inaf.it/extras/IGR/main.html

[3] XRT archival data are freely available at http://www.asdc.asi.it/

[4] Available at http://archive.eso.org/dss/dss

Table 1. Log of the spectroscopic observations presented in this paper (see text for details).

(1) Object	*(2)* RA (J2000)	*(3)* Dec (J2000)	*(4)* Telescope+instrument	*(5)* λ range (Å)	*(6)* Disp. (Å/pix)	*(7)* UT Date & Time at mid-exposure	*(8)* Exposure time (s)
IGR J00515−7328	00:52:00.59	−73:29:25.5	*Radcliffe*+Gr. Spec.	3750–7750	2.3	18 Nov. 2011, 19:17	2 × 1800
RX J0101.8−7223	01:01:52.28	−72:23:34.1	CTIO 1.5 m+RC Spec.	3300–10 500	5.7	24 Sep. 2011, 06:38	2 × 1200
IGR J02045−1156	02:04:36.75	−11:59:43.4	AAT+6dF	3900–7600	1.6	05 Dec. 2002, 10:52	1200+600
IGR J02115−4407	02:11:43.83*	−44:07:01.0*	CTIO 1.5 m+RC Spec.	3300–10 500	5.7	29 Dec. 2010, 03:48	3 × 1800
IGR J02447+7046‡	02:43:43.05	+70:50:38.5	TNG+DOLoReS	3700–8000	2.5	14 Sep. 2012, 02:48	1800
Swift J0250.2+4650	02:50:27.18	+46:47:29.4	SPM 2.1 m+B&C Spec.	3300–7900	4.0	04 Dec. 2008, 04:37	2 × 1800
IGR J02574−0303	02:57:22.10	−03:06:22.4	SPM 2.1 m+B&C Spec.	3300–7900	4.0	04 Dec. 2012, 05:37	2 × 1800
IGR J03564+6242	03:55:41.29	+62:40:56.7	TNG+DOLoReS	3700–8000	2.5	16 Sep. 2012, 02:35	1200
IGR J05048−7340	05:05:06.26	−73:39:04.3	CTIO 1.5 m+RC Spec.	3300–10 500	5.7	29 Dec. 2010, 06:49	2 × 1000
IGR J05470+5034	05:47:14.88	+50:38:25.5	*Copernicus*+AFOSC	3500–7800	4.2	01 Mar. 2011, 21:50	2 × 1800
IGR J06293−1359	06:29:20.22*	−13:55:23.9*	TNG+DOLoReS	3700–8000	2.5	26 Oct. 2011, 05:21	3 × 1800
IGR J09034+5329	09:03:05.51*	+53:30:32.5*	TNG+DOLoReS	3700–8000	2.5	30 Oct. 2011, 02:58	2 × 1500
Swift J0958.0−4208	09:57:50.64	−42:08:35.5	CTIO 1.5 m+RC Spec.	3300–10 500	5.7	06 Dec. 2010, 07:40	2 × 1500
IGR J10200−1436	10:19:37.29*	−14:41:28.3*	TNG+DOLoReS	3700–8000	2.5	05 Dec. 2011, 04:08	2 × 1200
IGR J14257−6117	14:25:07.58	−61:18:57.8	CTIO 1.5 m+RC Spec.	3300–10 500	5.7	26 Jan. 2012, 08:10	3 × 1800
IGR J14488−4008	14:48:50.97	−40:08:45.6	CTIO 1.5 m+RC Spec.	3300–10 500	5.7	02 Feb. 2012, 07:13	2 × 1000
IGR J15415−5029	15:41:26.43	−50:28:23.3	CTIO 1.5 m+RC Spec.	3300–10 500	5.7	21 Mar. 2012, 07:40	2 × 1200
IGR J16058−7253:							
LEDA 259433	16:05:23.24	−72:53:56.2	CTIO 1.5 m+RC Spec.	3300–10 500	5.7	15 May 2012, 07:56	2 × 1800
LEDA 259580	16:06:06.88	−72:52:41.9	CTIO 1.5 m+RC Spec.	3300–10 500	5.7	15 May 2012, 09:00	2 × 1500
IGR J17014−4306	17:01:28.15	−43:06:12.3	CTIO 1.5 m+RC Spec.	3300–10 500	5.7	02 Oct. 2011, 00:21	2 × 1000
IGR J17198−3020	17:19:48.65	−30:17:26.9	SPM 2.1 m+B&C Spec.	3300–7900	4.0	23 Jun. 2012, 06:00	1800
IGR J17476−2253	17:47:29.80**	−22:52:46.6**	TNG+DOLoReS	3700–8000	2.5	11 Jul. 2012, 02:45	2 × 1800
IGR J17488−2338	17:48:39.05**	−23:35:21.2**	TNG+DOLoReS	3700–8000	2.5	25 Aug. 2012, 01:39	2 × 1800
IGR J17520−6018	17:51:55.80	−60:19:43.2	CTIO 1.5 m+RC Spec.	3300–10 500	5.7	24 Sep. 2011, 01:36	2 × 1000
IGR J18151−1052	18:15:03.8†	−10:51:35†	TNG+DOLoReS	3700–8000	2.5	02 Aug. 2011, 22:00	2 × 1500
IGR J18256−1035	18:25:43.83**	−10:35:01.3**	TNG+DOLoReS	3700–8000	2.5	21 Ago 2011, 23:20	2 × 1800
AX J1832.3−0840	18:32:19.30*	−08:40:29.8*	SPM 2.1 m+B&C Spec.	3300–7900	4.0	24 Jun. 2012, 08:19	2 × 1800
2E 1923.7+5037	19:25:02.17	+50:43:13.8	*Cassini*+BFOSC	3500–8700	4.0	21 Aug. 2012, 21:10	2 × 1800
IGR J19295−0919‡	19:29:04.02**	−09:13:42.9**	TNG+DOLoReS	3700–8000	2.5	02 Sep. 2011, 01:41	1800
IGR J21319+3619‡	21:31:27.37*	+36:16:50.2*	TNG+DOLoReS	3700–8000	2.5	18 Aug. 2012, 03:15	2 × 1800
IGR J21565+5948‡	21:56:04.18	+59:56:04.5	TNG+DOLoReS	3700–8000	2.5	03 Aug. 2011, 03:29	2 × 1500
IGR J22534+6243	22:53:55.12	+62:43:36.8	SPM 2.1 m+B&C Spec.	3300–7900	4.0	22 Jun. 2012, 11:07	2 × 900
IGR J23558−1047	23:55:58.82*	−10:46:44.8*	SPM 2.1 m+B&C Spec.	3300–7900	4.0	26 Sep. 2011, 07:23	2 × 1200

Notes. If not indicated otherwise, source coordinates were extracted from the 2MASS catalogue and have an accuracy better than 0.″1. (‡) Sources for which the 99% IBIS error circle was considered to search for a soft X-ray counterpart. (*) Coordinates extracted from the USNO catalogues, having an accuracy of about 0.″2 (Deutsch 1999; Assafin et al. 2001; Monet et al. 2003). (**) Coordinates computed through astrometry calibrated using the USNO catalogues on a previously acquired image of the source field (see text). (†) Coordinates extracted from the DSS-II-Red frames having an accuracy of ∼1″.

to be followed up with optical spectroscopy (e.g., Landi et al. 2010 and Tomsick et al. 2012).

Finally, another consistency check concerning the objects from Bird et al. (2010) was performed using more recent IBIS maps to see if the selected hard X-ray sources are still detected with INTEGRAL. Indeed, all of them were recovered with the possible exceptions of IGR J17198−3020 and IGR J21319+3619, which however appear to display a high value for the associated "bursticity" parametre (see details in Bird et al. 2010), thus indicating substantial hard X-ray variability.

In this way, we collected a sample of 32 INTEGRAL objects with possible optical counterparts, which we explored by means of optical spectroscopy. Their names and accurate coordinates (to 1″ or better; see next section) are reported in Table 1, while their optical finding charts are shown in Figs. 1–4 with the corresponding putative counterparts indicated with tick marks. We did not report the chart that corresponds to IGR J18151−1052, as it already appears in Lutovinov et al. (2012).

It is stressed that sources IGR J17476−2253 (Mescheryakov et al. 2009), IGR J18151−1052 (Lutovinov et al. 2012) and IGR J21565+5948 (Bikmaev et al. 2010) are also included in our final sample. Although already identified elsewhere, these objects still have fragmentary longer-wavelength information. Our observations are thus presented here to confirm their nature and to improve their classification and characteristics.

Within this selection, we were also able to determine the actual counterpart of source IGR J06293−1359, which in Paper VIII was tentatively (and, in hindsight, erroneously) identified with a Seyfert 2 AGN on the basis of an association with a radio object inside the hard X-ray error box of this source. This occurred as no soft X-ray observations of the field were available at that time. We also refer the reader to Paper III concerning the caveats and the shortcomings of choosing sources that are not straightforwardly connected with an arcsec-sized soft X-ray position within an IBIS uncertainty circle.

For the source naming in Table 1, we directly adopted the names as they appear in the relevant works (Bird et al. 2010; Bottacini et al. 2012; Ricci et al. 2012; Coe et al. 2010; Grebenev et al. 2013; Krivonos et al. 2010, 2012), and the IGR alias when available. However, we remark that we chose not to use the ROSAT name as reported in the fourth IBIS Survey (Bird et al. 2010) for one of the selected objects (1RXS J090320.0+533022), because the soft X-ray emission detected with *Swift*/XRT within the corresponding 90% IBIS error circle is not positionally consistent with the one reported in the ROSAT Faint Catalogue (actually, no detectable emission appears to be associated with this ROSAT object from

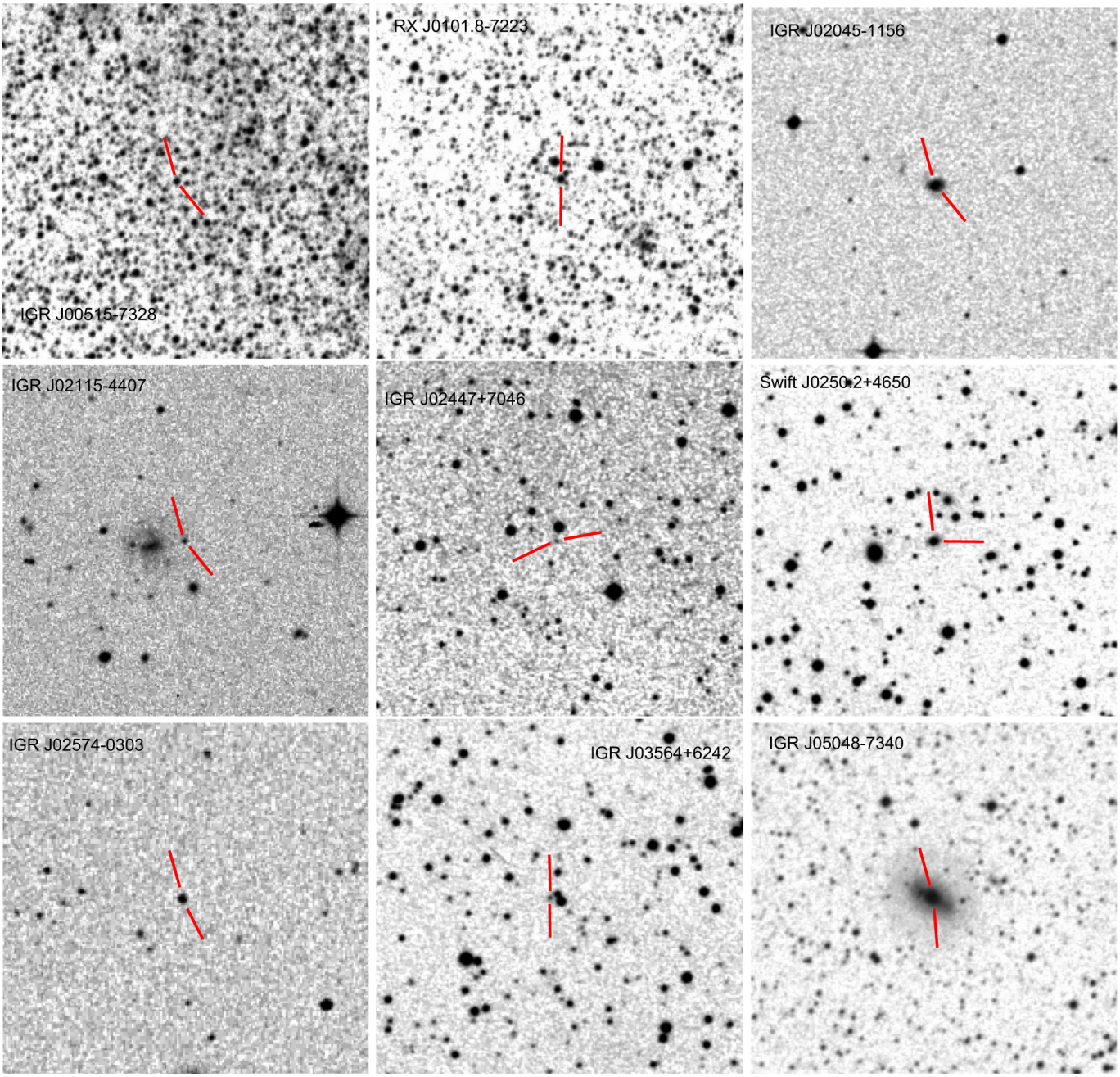

Fig. 1. Optical images of the fields of nine INTEGRAL hard X-ray sources selected in this paper for optical spectroscopic follow-up (see Table 1). The object name is indicated in each panel. The proposed optical counterparts are indicated with tick marks. Field sizes are $5' \times 5'$. Nearly all mages were extracted from the DSS-II-Red survey; the one for IGR J02574−0303 (*bottom left panel*) was instead obtained from the DSS-I-Blue survey. In all cases, north is up and *east to the left*.

the XRT images). Thus, we decided to rename this source as IGR J09034+5329 following the usual naming convention for sources detected with INTEGRAL.

3. Optical observations

Analogously to Papers VI-IX, almost all of the data presented in this work were secured during an observational campaign, which spanned over four years (from December 2008 to December 2012) and which involved the use of the following telescopes:

- the 1.5 m at the Cerro Tololo Interamerican Observatory (CTIO), Chile;
- the 1.52 m *Cassini* telescope of the Astronomical Observatory of Bologna, in Loiano, Italy;
- the 1.82 m *Copernicus* telescope of the Astronomical Observatory of Asiago, Italy;
- the 1.9 m *Radcliffe* telescope of the South African Astronomical Observatory (Sutherland, South Africa);
- the 2.1 m telescope of the Observatorio Astronómico Nacional in San Pedro Mártir (SPM), Mexico;
- the 3.58 m Telescopio Nazionale *Galileo* (TNG) at the Roque de Los Muchachos Observatory in La Palma, Spain.

The spectroscopic data acquired at these telescopes have been optimally extracted (Horne 1986) and reduced following

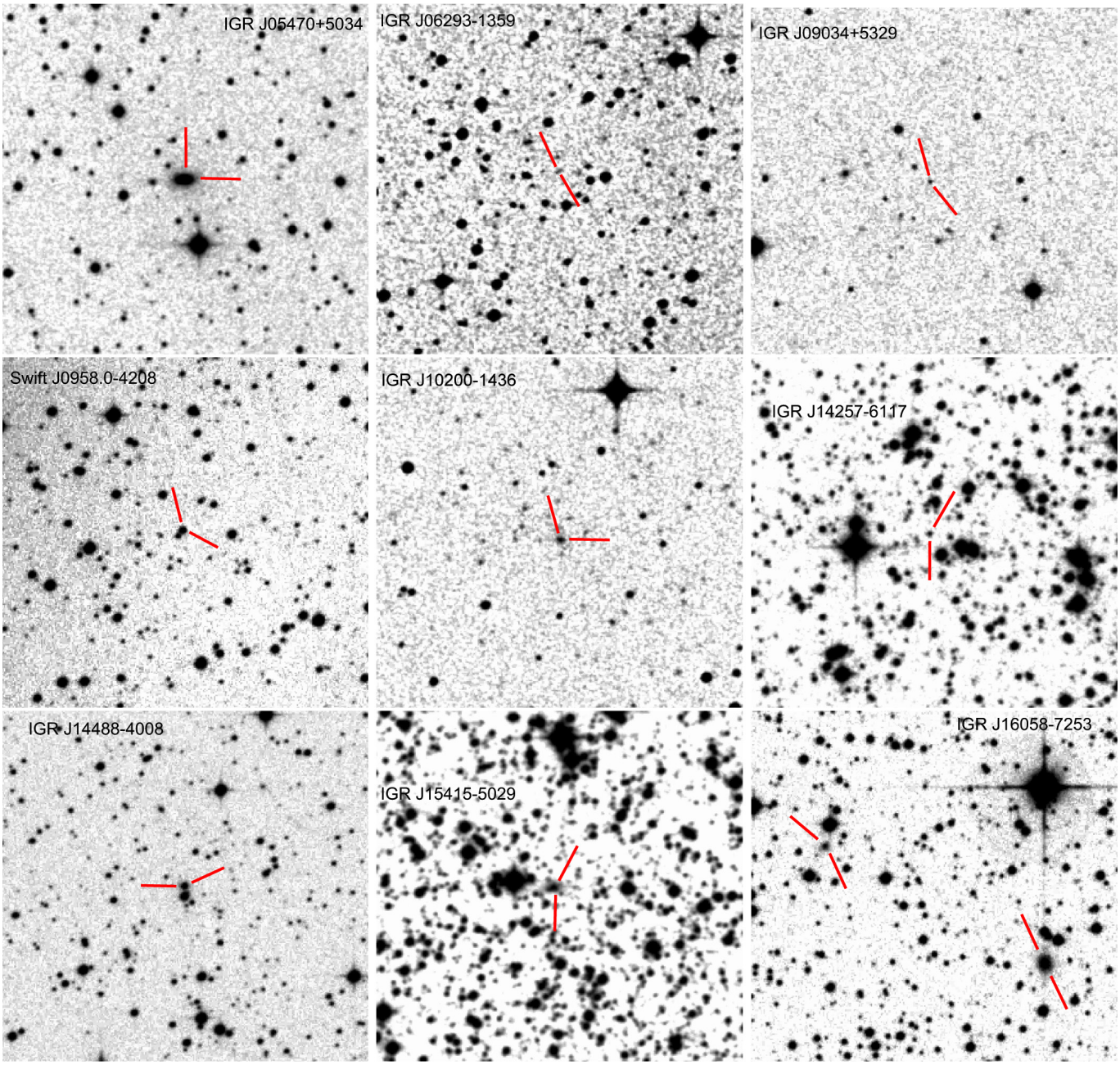

Fig. 2. Similar to Fig. 1 but for nine more INTEGRAL sources of our sample (see Table 1). For IGR J16058−7253 (*bottom right panel*), we indicate the two optical objects likely responsible for the total hard X-ray emission detected for this source (see Landi et al. 2012b and Sect. 4.1 of this paper).

standard procedures using IRAF[5]. Calibration frames (flat fields and bias) were taken on the day preceeding or following the observing night. The wavelength calibration was performed using lamp data acquired soon after each on-target spectroscopic acquisiton; the uncertainty in this calibration was ∼0.5 Å in all cases according to our checks that used the positions of background night sky lines. Flux calibration was obtained using catalogued spectrophotometric standards. Finally, the data of a given object were stacked together to increase the S/N when multiple spectra were acquired.

The spectrum of the optical counterpart of IGR J02045−1156 was instead retrieved from the Six-degree Field Galaxy Survey[6] (6dFGS) archive (Jones et al. 2004), acquired using the 3.9 m Anglo-Australian Telescope of the Australian Astronomical Observatory in Siding Spring (Australia). Since the 6dFGS archive contains spectra that are not calibrated in flux, we considered the optical photometric information in Jones et al. (2005) to calibrate the spectrum of this source.

In Table 1, we show a detailed log of all the spectroscopic observations presented in this paper. Column 1 indicates the names of the observed INTEGRAL sources. In Cols. 2 and 3, we list the equatorial coordinates of the proposed optical counterpart,

[5] IRAF is the Image Reduction and Analysis Facility made available to the astronomical community by the National Optical Astronomy Observatories, which are operated by AURA, Inc., under contract with the U.S. National Science Foundation. It is available at http://iraf.noao.edu/

[6] http://www.aao.gov.au/local/www/6df/

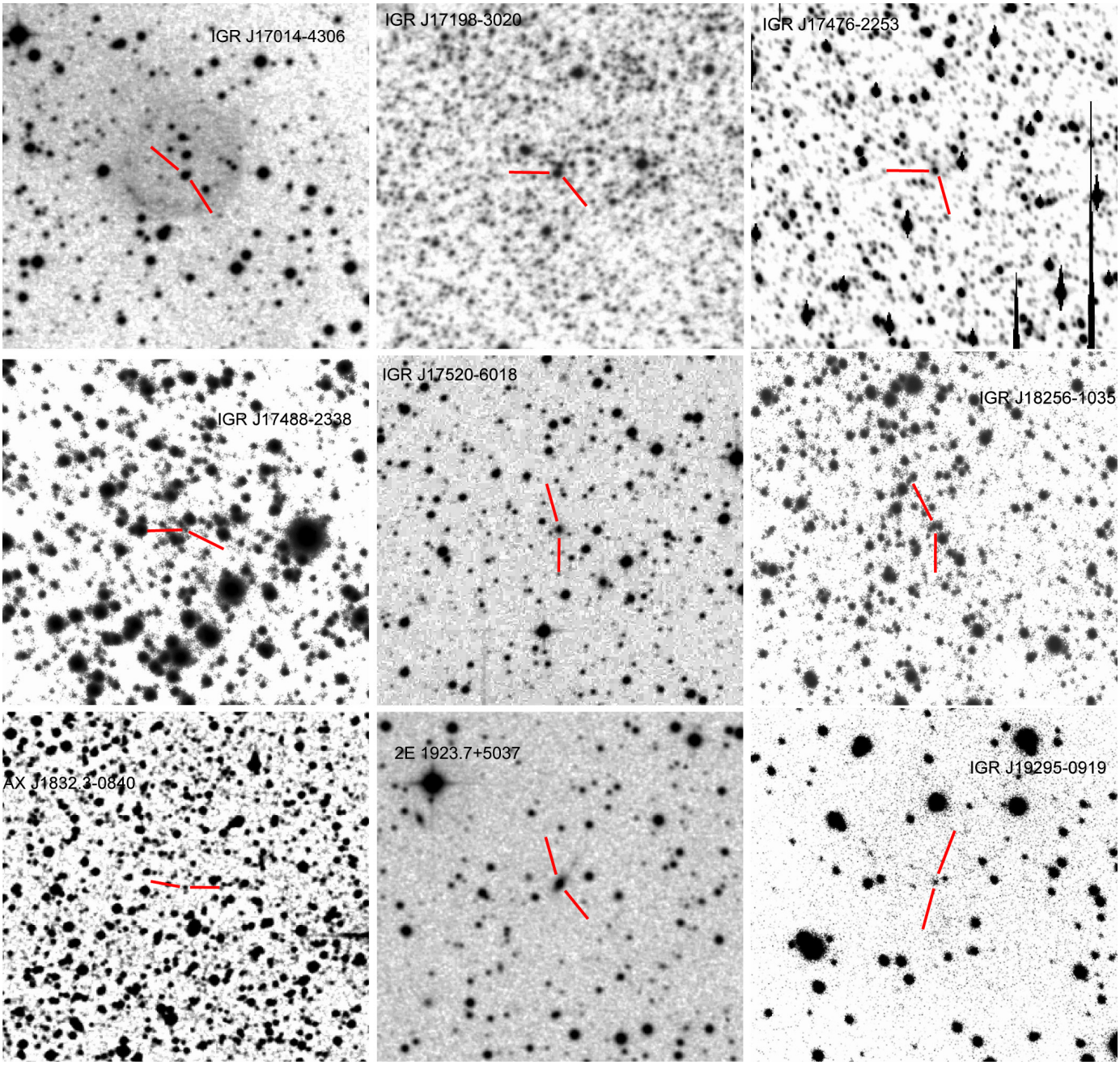

Fig. 3. Similar to Fig. 1 but for nine more INTEGRAL sources of our sample (see Table 1). The images of the fields of sources IGR J17476−2253, IGR J17488−2338, IGR J18256−1035 and IGR J19295−0919 were acquired with TNG+DOLoReS (see Table 2 for details) and cover an area of $1' \times 1'$.

mostly extracted from the 2MASS (with an uncertainty of $\leq 0\farcs1$: Skrutskie et al. 2006) or the USNO catalogues (with accuracies of about $0\farcs2$: Deutsch 1999; Assafin et al. 2001; Monet et al. 2003). The telescope and instrument used for the observations are reported in Col. 4, while characteristics of each spectrograph are presented in Cols. 5 and 6. Column 7 reports the observation date and the UT time at mid-exposure, and Col. 8 provides the exposure times and the number of observations for each source.

Before engaging in spectroscopic observations, for four cases (see Table 2) we acquired a deeper and higher resolution image of the corresponding field with respect to that available from the DSS-II-Red survey. All images were acquired with TNG+DOLoReS, which covers a field of $8\farcm6 \times 8\farcm6$ with a scale of $0\farcs252$ pix^{-1}. These were then processed to obtain an astrometric solution based on USNO-A2.0[7] reference stars in each field. The conservative error in the optical positions can be assumed as

Table 2. Log of the optical images acquired with TNG+DOLoReS and used to perform the astrometric calibration of the field of selected sources belonging to our sample (see also Fig. 2).

Object	Date and time (UT)	T_{exp} (s)	Filter	Seeing
IGR J17476−2253	21 Jun. 2012, 03:15	300	*R*	$0\farcs9$
IGR J17488−2338	01 Sep. 2010, 20:55	5	open	$1\farcs2$
IGR J18256−1035	21 Aug. 2011, 22:46	5	open	$0\farcs9$
IGR J19295−0919	22 Aug. 2011, 00:00	10	open	$1\farcs0$

[7] Available at: http://archive.eso.org/skycat/servers/usnoa

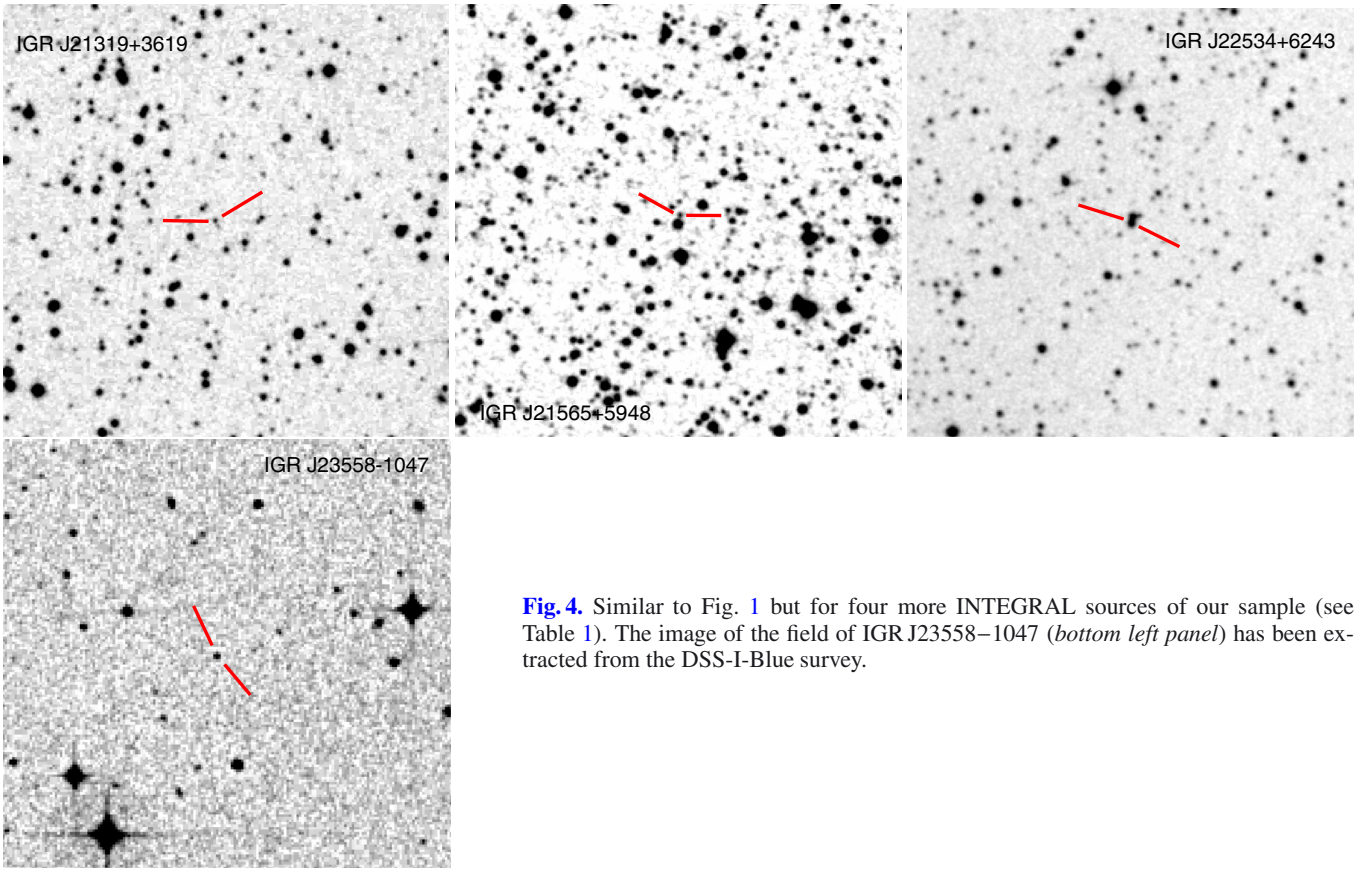

Fig. 4. Similar to Fig. 1 but for four more INTEGRAL sources of our sample (see Table 1). The image of the field of IGR J23558−1047 (*bottom left panel*) has been extracted from the DSS-I-Blue survey.

0.″252, which was then added in quadrature to the systematic error in the USNO-A2.0 catalogue. For these images, the final 1σ uncertainty in the astrometric solution is thus 0.″35: this can be considered the error in the coordinates of the optical counterparts of the INTEGRAL sources listed in Table 2 (see also Table 1).

With the exception of the field of IGR J17476−2253, the above images were acquired in white light (that is, with no filter), so no meaningful determination of the magnitude of the corresponding optical counterpart could be obtained. For the case of IGR J17476−2253, we attempted an estimate of the optical counterpart *R*-band magnitude by using the photometry zero-points available for DOLoReS[8]. This approach was chosen given that no reliable calibrator was available in the image, as all USNO-A2.0 stars with a catalogued *R*-band magnitude and close to the position of the optical counterpart of this INTEGRAL source were saturated in the TNG acquisition image. Despite the crowdedness of the field (see Fig. 3, upper right panel), we used simple aperture photometry because the object is apparently extended, so the application of the standard point spread function fitting technique was not viable.

4. Results

A full description of the adopted identification and classification criteria for the optical spectra of the selected sources can be found in our previous papers (I–IX); the reader is thus referred to them for details. The optical magnitudes quoted below, when not stated otherwise, are extracted from the USNO-A2.0 catalogue. We briefly recall here that the main criteria used for the classification of AGN spectra are from Veilleux & Osterbrock (1987), Winkler (1992), Ho et al. (1993, 1997) and Kauffmann et al. (2003).

To estimate the reddening along the line of sight for the Galactic sources in our sample when possible and applicable, we assumed an intrinsic H_α/H_β line ratio of 2.86 (Osterbrock 1989) and inferred the corresponding color excess by comparing the intrinsic line ratio with the measured one by applying the Galactic extinction law of Cardelli et al. (1989) and the total-to-selective extinction ratio of Rieke & Lebofsky (1985).

To evaluate the distances of the compact Galactic X-ray sources of our sample, we assumed an absolute magnitude $M_V \sim +9$ and an intrinsic color index $(V-R)_0 \sim 0$ mag (Warner 1995) for cataclysmic variables (CVs), whereas we used the intrinsic stellar color indices and absolute magnitudes from Lang (1992) and Wegner (1994) for high-mass X-ray binaries (HMXBs). Although these approaches basically provide an approximate value for the distance of Galactic sources, our past experience (Papers I-IX) tells us that these estimates can be considered correct to within 50% of the refined value subsequently determined with more precise measurements.

For extragalactic sources, we assume a cosmology with $H_0 = 65$ km s^{-1} Mpc^{-1}, $\Omega_\Lambda = 0.7$, and $\Omega_m = 0.3$; the luminosity distances of the extragalactic objects presented in this paper were determined for these parametres using the Cosmology Calculator of Wright (2006). When not explicitly stated otherwise, we assume a Crab-like spectrum in our X-ray flux estimates except for the catalogued *XMM-Newton* sources, for which we considered the fluxes reported in Saxton et al. (2008) or in Watson et al. (2009). The X-ray luminosities reported in Tables 3, 4, 5, 7, 8, and 9 are associated with a letter indicating the satellite and/or the instrument, namely ASCA (*A*), *Swift*/BAT (*B*), *Chandra* (*C*), *Einstein* (*E*), INTEGRAL (*I*),

[8] See Table 2 at http://www.tng.iac.es/instruments/lrs/

Table 3. Synoptic table containing the main results for the seven high-redshift QSOs ($z > 0.5$; Figs. 5 and 6) identified in the present sample of INTEGRAL sources.

Object	$F_{[OII]}$	F_{MgII}	$F_{CIII]}$	F_{CIV}	z	D_L (Mpc)	$E(B-V)_{Gal}$	L_X
IGR J02115−4407	–	9.5 ± 1.0	6.6 ± 0.6	–	1.212	9025.9	0.017	150 (20–40; *I*)
	–	[10.0 ± 1.0]	[12.4 ± 01.2]	–				<220 (40–100; *I*)
IGR J03564+6242	–	5.7 ± 0.5	1.4 ± 0.4	–	1.109	8086.6	0.910	2.0 (2–10; *X*)
	–	[54 ± 5]	[6 ± 2]	–				190 (20–100; *I*)
IGR J09034+5329	–	2.9 ± 0.3	2.9 ± 0.3	–	1.253	9405.2	0.015	180 (20–40; *I*)
	–	[3.0 ± 0.3]	[3.0 ± 0.3]	–				<270 (40–100; *I*)
IGR J16388+3557	–	–	4.5 ± 0.5	1.9 ± 0.3	2.020	16 936.9	0.021	750 (20–100; *I*)
	–	–	[5.0 ± 0.5]	[2.0 ± 0.3]				
IGR J21319+3619	–	2.4 ± 0.2	1.40 ± 0.15	2.3 ± 0.2	1.488	11 631.4	0.212	<50 (20–40; *I*)
	–	[3.2 ± 0.3]	[2.8 ± 0.3]	[5.7 ± 0.6]				<90 (40–100; *I*)
IGR J23558−1047	–	4.9 ± 0.5	–	–	1.108	8077.6	0.034	0.66 (2–10; *X*)
	–	[5.0 ± 0.5]	–	–				480 (20–100; *I*)
IGR J19295−0919	0.65 ± 0.03	–	–	–	0.741	4918.3	0.292	50 (20–100; *I*)
	[1.32 ± 0.07]	–	–	–				

Notes. The upper part deals with the Type 1 QSOs of the sample, while the lower part with the single Type 2 QSO identified in this paper. Emission-line fluxes are reported both as observed and (between square brackets) corrected for the intervening Galactic absorption $E(B-V)_{Gal}$ along the object line of sight (from Schlegel et al. 1998). Line fluxes are in units of 10^{-15} erg cm^{-2} s^{-1}, X-ray luminosities are in units of 10^{45} erg s^{-1}, and the reference band (between round brackets) is expressed in keV. In the last column, the upper case letter indicates the satellite and/or the instrument with which the corresponding X-ray flux measurement was obtained (see text). The typical error of the redshift measurement is ±0.001 except for the spectrum of IGR J16388+3557, for which an uncertainty of ±0.005 is assumed.

Table 4. Synoptic table containing the main results for the eight low-z broad emission-line AGNs (Fig. 7) identified or observed in the present sample of INTEGRAL sources.

Object	F_{H_β}	$F_{[OIII]}$	Class	z	D_L (Mpc)	$E(B-V)_{Gal}$	L_X
IGR J02447+7046	2.0 ± 0.2	0.66 ± 0.06	Sy1.2	0.306	1710.8	0.770	3.7 (20–100; *I*)
	[11.6 ± 1.2]	[3.9 ± 0.4]					
IGR J02574−0303	5.5 ± 0.6	1.51 ± 0.15	Sy1.2	0.197	1037.8	0.047	0.13 (0.5–10; *X*)
	[5.6 ± 0.6]	[1.63 ± 0.16]					2.6 (17–80; *I*)
IGR J06293−1359	0.47 ± 0.07	0.31 ± 0.03	Sy1.5	0.376	2174.8	0.317	9.6 (20–40; *I*)
	[1.2 ± 0.2]	[0.62 ± 0.06]					<7.9 (40–100; *I*)
IGR J14488−4008	120 ± 20	45 ± 4	Sy1.2	0.123	619.0	0.109	0.11 (2–10; *X*)
	[160 ± 30]	[58 ± 6]					0.17 (20–40; *I*)
							<0.17 (40–100; *I*)
							0.33 (17–60; *I*)
							0.60 (14–195; *B*)
							0.38 (15–150; *B*)
IGR J17476−2253	6.0 ± 0.6	5.73 ± 0.17	Sy1.5	0.047	224.5	1.009	0.016–0.030 (2–10; *X*)
	[127 ± 13]	[121 ± 4]					0.11 (20–100; *I*)
							0.060 (17–60; *I*)
							0.11 (14–195; *B*)
							0.090 (15–150; *B*)
IGR J17488−2338	1.08 ± 0.16	1.13 ± 0.03	Sy1.5	0.240	1295.7	1.570	0.70 (0.2–12; *N*)
	[62 ± 9]	[54.8 ± 1.6]					0.46 (2–10; *X*)
							2.8 (20–100; *I*)
2E 1923.7+5037	137 ± 10	27.9 ± 1.4	Sy1.2	0.068	329.8	0.093	0.013 (0.1–2.4; *X*)
	[173 ± 12]	[36.1 ± 1.8]					0.014 (0.16–3.5; *E*)
							0.13 (0.2–12; *N*)
							0.10 (18–55; *I*+*B*)
							0.13 (14–195; *B*)
IGR J21565+5948	0.55 ± 0.06	2.8 ± 0.4	Sy1	0.209	1108.7	1.267	0.010 (0.1–2.4; *R*)
	[68 ± 10]	[13.7 ± 1.4]					0.21 (0.3–10; *C*)
							0.18 (2–10; *X*)
							1.4 (20–100; *I*)

Notes. Emission-line fluxes are reported both as observed and (between square brackets) corrected for the intervening Galactic absorption $E(B-V)_{Gal}$ along the object line of sight (from Schlegel et al. 1998). Line fluxes are in units of 10^{-15} erg cm^{-2} s^{-1}, X-ray luminosities are in units of 10^{45} erg s^{-1}, and the reference band (between round brackets) is expressed in keV. In the last column, the upper case letter indicates the satellite and/or the instrument with which the corresponding X-ray flux measurement was obtained (see text). The typical error of the redshift measurement is ±0.001.

Table 5. Synoptic table containing the main results for the seven low-redshift narrow emission-line AGNs (Fig. 8) and for the two XBONGs (Fig. 9) identified or observed in the present sample of INTEGRAL sources.

Object	$F_{H\alpha}$	$F_{H\beta}$	$F_{[OIII]}$	Class	z	D_L	$E(B-V)$		L_X
						(Mpc)	Gal.	AGN	
IGR J02045−1156	196 ± 10 [196 ± 10]	32 ± 3 [35 ± 4]	31 ± 3 [33 ± 3]	LINER	0.0727	353.7	0.023	0.68	0.61 (0.1–2.4; *R*) 4.3 (0.2–12; *N*) 1.4 (0.3–10; *X*) 24 (17–80; *I*)
Swift J0250.2+4650	31.4 ± 1.6 [48 ± 3]	6.5 ± 0.7 [13.7 ± 1.4]	67 ± 2 [124 ± 4]	Sy2	0.021	98.4	0.194	0.20	0.20 (0.2–12; *N*) 1.7 (17–60; *I*) 2.3 (14–195; *B*) 2.0 (15–150; *B*)
IGR J05048−7340	in abs. [in abs.]	in abs. [in abs.]	<8 [<12]	XBONG	0.014	69.0	0.127	–	0.31 (20–60; *I*) 0.48 (14–195; *B*) 0.43 (15–150; *B*)
IGR J05470+5034	29 ± 3 [48 ± 5]	3.4 ± 1.0 [7 ± 2]	20 ± 2 [40 ± 4]	Sy2	0.036	170.6	0.233	0.83	0.006 (0.1–2.4; *R*) 5.9 (17–60; *I*) 8.3 (14–195; *B*) 5.6 (15–150; *B*)
IGR J10200−1436	– –	<0.03 [<0.05]	<0.07 [<0.08]	XBONG	0.391	2277.2	0.104	–	6.8 (0.1–2.4; *X*) 740 (20–40; *I*) <810 (40–100; *I*)
IGR J15415−5029	12.1 ± 1.8 [86 ± 13]	<0.17 [<13]	4.7 ± 0.7 [66 ± 10]	likely Sy2	0.032	151.2	0.862	>0.85	0.15 (0.3–10; *C*) 1.7 (17–60; *I*) 3.0 (20–100; *I*) 2.5 (15–150; *B*)
IGR J16058−7253*									
(LEDA 259433)	4.6 ± 0.5 [8.5 ± 0.9]	in abs. [in abs.]	7.6 ± 0.7 [9.4 ± 0.9]	likely Sy2	0.069	334.8	0.094	–	4.4 (2–10; *X*)
(LEDA 259580)	5.7 ± 0.5 [6.4 ± 0.6]	<2 [<3]	7.8 ± 0.8 [1.05 ± 0.11]	Sy2	0.090	373.0	0.094	>0	4.8 (2–10; *X*)
IGR J17520−6018	2.7 ± 0.8 [3.2 ± 0.9]	in abs. [in abs.]	4.4 ± 1.1 [5.4 ± 1.4]	likely Sy2	0.112	559.6	0.091	–	9.7 (2–10; *X*) 86 (20–100; *I*) 56 (14–195; *B*)

Notes. Emission-line fluxes are reported both as observed and (between square brackets) corrected for the intervening Galactic absorption $E(B-V)_{Gal}$ along the object line of sight (from Schlegel et al. 1998). Line fluxes are in units of 10^{-15} erg cm^{-2} s^{-1}, X-ray luminosities are in units of 10^{43} erg s^{-1}, and the reference band (between round brackets) is expressed in keV. In the last column, the upper case letter indicates the satellite and/or the instrument with which the corresponding X-ray flux measurement was obtained (see text). The typical error of the redshift measurement is ±0.001 except for the 6dFGS spectrum of IGR J02045−1156, for which an uncertainty of ±0.0003 can be assumed. (*) We did not attempt to estimate the total hard X-ray luminosity of IGR J16058−7253 and the contributions of the two AGNs to this quantity due to the lack of information on their X-ray spectra.

XMM-Newton (*N*), ROSAT (*R*), and *Swift*/XRT (*X*), with which the measurement of the corresponding X-ray flux was obtained.

In the following, we present the object identifications by dividing them into four broad classes (AGNs, X-ray binaries, CVs, and active stars) as we did in some of our previous papers.

4.1. AGNs

It is found that 23 objects in our sample have optical spectra that allow their classification as AGNs (see Figs. 4–8). The majority of them exhibits redshifted broad and/or narrow emission lines typical of nuclear galactic activity: 13 sources can be classified as Type 1 (broad-line) and eight as Type 2 (narrow-line) AGNs.

In addition, two X-ray objects (IGR J05048−7340 and IGR J10200−1436) are associated with galaxies showing absorption features only (see Fig. 9). Using the approach of Laurent-Muehleisen et al. (1998), we find that these sources do not show any suggestion of AGN activity: we thus classify them as X-ray bright, optically normal galaxies (XBONGs; see Comastri et al. 2002). We also note that we identify IGR J10200−1436 as the farthest XBONG known up to now within the hard X-ray surveys made with INTEGRAL.

Moreover, we remark that 6 AGNs (5 broad-line and one narrow-line) identified here are found with a high redshift ($z > 0.5$; see Table 3). In particular, all broad-line cases lie at $z > 1$; we also identify a narrow-line hard X-ray emitting AGN at high redshift (IGR J19295−0919; see below).

The division of low-redshift Type 1 AGNs in terms of subclasses is reported in Table 4. In this same table we do not report the fluxes of the broad H_α emission because it is heavily blended with other emission lines (mainly [N II]) in all cases.

The main observed and inferred parametres for each of these broad classes of AGNs are displayed in Tables 3–5. In these tables, X-ray luminosities were computed from the fluxes reported in McDowell (1994), Voges et al. (1999, 2000), ROSAT Team (2000), Saxton et al. (2008), Rodriguez et al. (2009), Bird et al. (2010), Cusumano et al. (2010), Landi et al. (2010, 2012b), Maiorano et al. (2010), Malizia et al. (2011, 2012a), Bottacini et al. (2012), Krivonos et al. (2012), Molina et al. (2012a,b), Ricci et al. (2012), Tomsick et al. (2012), Baumgartner et al. (2013), and Grebenev et al. (2013).

In this paper, we also report the redshift value for most AGNs of our sample (18 out of 23) for the first time. Among them, we confirm and refine the value for the photometric redshift

Table 6. BLR gas velocities (in km s^{-1}), central black hole masses (in units of 10^8 $M_\odot$), and apparent Eddington ratios for the 14 broad line AGNs discussed in this paper.

Object	$v_{\rm BLR}$	$M_{\rm BH}$	$L_X/L_{\rm Edd}$
IGR J02447+7046	4000	1.4	0.2
IGR J02574−0303	3900	0.42	~0.5
IGR J06293−1359	5700	0.87	<1.6
IGR J14488−4008	5300	3.8	<0.007
IGR J17476−2253	11 100	3.6	0.002
IGR J17488−2338	8200	13	<0.006
2E 1923.7+5037	9700	5.8	~0.002
IGR J21565+5948	5700	5.6	0.02
IGR J02115−4407	6100	8.9	<3.3
IGR J03564+6242	11 300	63	0.2
IGR J09034+5329	11 000	20	<1.8
IGR J21319+3619	10 700	19	<0.6
IGR J23558−1047	8200	11	3.5
IGR J16388+3557	23000	160	0.4

Notes. The final uncertainties on the black hole mass estimates are about 50% of their values. The velocities were determined using H_β, Mg II, or C IV emissions (upper, central and lower part of the table, respectively), whereas the apparent Eddington ratios were computed using the (observed or rescaled, see text) 20–100 keV luminosities.

($z = 1.1$) of the optical counterpart of IGR J23558−1047 proposed by Richards et al. (2009). The redshifts of the remaining five cases are compatible with those reported in the literature (Paturel et al. 2003; Mescheryakov et al. 2009; Bikmaev et al. 2010). We moreover give a more accurate classification for IGR J17476−2253 in terms of Seyfert 1.5 galaxy (the source was previously identified by Mescheryakov et al. 2009 as a Seyfert 1 AGN).

We take this opportunity to correct and/or improve the following points. First, we give (see Table 4) the correct identification for the actual optical counterpart of IGR J06293−1359 (in Fig. 7) as a Seyfert 1.5 galaxy at $z = 0.376$; the tentative identification given in Paper VIII should thus be discarded for the reasons given in Sect. 2 above. Next, we correct the line identifications (given in Paper IX) in the spectrum of the optical counterpart of IGR J16388+3557 as shown in Fig. 6. This leads to a corrected redshift $z = 2.020$ (see Table 3).

We moreover revise the AGN class of galaxy LEDA 7910, proposed as the optical counterpart of IGR J02045−1156 (Ricci et al. 2012). The presence of pure narrow emission lines in its spectrum (Fig. 8, upper left panel) is at variance with the (intermediate) Seyfert 1 spectrum and classification reported by Augarde et al. (1994). Rather, we classify it as a LINER (Heckman 1980) on the basis of its emission line ratios in the spectrum presented here. This indicates that this source changed its spectral appearance between the late 1980s and the 6dFGS observation of December 2002.

Let us now focus on the optical and X-ray properties of other interesting AGN sources within our sample.

First, we would like to draw the reader's attention on the spectrum of the optical counterpart of IGR J19295−0919 (Fig. 5, bottom right panel). Although the high-z nature of this source does not allow us to apply the emission line ratio diagnostics for the AGN classification (all relevant lines lie in the infrared bands in the observer's frame), we can nevertheless classify the object as a Type 2 (i.e., narrow-line) QSO due to the large X-ray luminosity, which is at least four orders of magnitude larger than that of the brightest starbursts (David et al. 1992). Only five objects of this kind were detected up to now with INTEGRAL (Malizia et al. 2012b); IGR J19295−0919 is the sixth and farthest one, being located at redshift $z = 0.741$.

Figure 7 reports the spectra of the low-redshift ($z < 0.5$) broad-line AGNs in our sample. It is noteworthy that two of them, IGR J17476−2253 and 2E 1923.7+5037, show double-peaked Balmer lines in emission (this is particularly evident in the case of the H_α line for both objects). This characteristic is not frequent in the optical spectra of broad-line AGNs and may indicate asymmetries in their broad-line region (BLR), such as an elliptical disk, warps, spiral shocks, or hot spots (Strateva et al. 2003), or a lower accretion rate with respect to AGNs with single-peaked broad emissions (Eracleous & Halpern 1994; Ho et al. 2000).

The value for the R-band magnitude of the optical counterpart of IGR J17476−2253 extracted from the field image of this source is reported here. Considering all the caveats described in Sect. 3, we obtained a magnitude $R = 18.4 \pm 0.3$ for the optical counterpart of IGR J17476−2253, where the large error mainly reflects the systematic uncertainties of the photometry. This value is broadly consistent with that reported by Mescheryakov et al. (2009).

Regarding IGR J16058−7253, we confirm the suggestion of Landi et al. (2012b) that this hard X-ray emission is the sum of the contributions of two narrow-line AGNs within the IBIS error circle of the source but at different redshifts (see Table 5). By applying the statistical approach of Tomsick et al. (2012) and using the X-ray fluxes of Landi et al. (2012b), we see that the probability for each of the two X-ray emitting galaxies, LEDA 259433 and LEDA 259580, that can be contained by chance in the hard X-ray error circle is less than 3×10^{-3} with a slight dependence on the chosen error size (Cusumano et al. 2010; Krivonos et al. 2012; Baumgartner et al. 2013). This further strengthens the above mentioned indication of Landi et al. (2012b) and makes this hard X-ray object similar to the case of IGR J20286+2544, which is most likely the combined high-energy emission of two X-ray variable AGNs (Paper IV; Winter et al. 2008). In Table 5, we did not attempt to evaluate either the total hard X-ray luminosity of IGR J16058−7253 or the contributions of the two AGNs to this quantity due to the present lack of an accurate model of their X-ray spectra.

We also point out that Molina et al. (2012b) reports the presence of two soft X-ray sources within the IBIS error circle of IGR J14488−4008. Our identification as a Seyfert 1.2 galaxy (LEDA 589690) corresponds to the brighter of the two X-ray objects (the one labelled as "N1" by Molina et al. 2012b). Indeed, we also acquired an optical spectrum of source "N2" of Molina et al. (2012b) with the 1.5 m CTIO telescope on 2 February 2012 and found that it is a G-type Galactic star with no peculiarities. Likewise, source #2 of Malizia et al. (2011) in the field of IGR J23558−1047 (though formally outside the 90% IBIS error circle) was observed by us from Loiano on 22 August 2011 and again shows the optical spectrum of a normal star of G type. Source #1 of Landi et al. (2010) in the error circle of IGR J21565+5948 was spectroscopically confirmed as a normal A-type star by Bikmaev et al. (2010). Therefore, we will not discuss these objects further. In a similar vein, we focused our attention on LEDA 3077397 following the statistical considerations of Tomsick et al. (2012) with regard to the putative optical counterpart of IGR J15415−5029.

We now consider the Type 2 galaxies for which an estimate of the absorption local to the AGN is possible, and we apply the diagnostic T of Bassani et al. (1999) to their cases, i.e. the ratio

Table 7. Main results for the X-ray binaries (see Fig. 10) identified in the present sample of INTEGRAL sources.

Object	H_α		H_β		R	A_V	d	Spectral	L_X
	EW	Flux	EW	Flux	mag	(mag)	(kpc)	type	
IGR J00515−7328	4.5 ± 0.6	8.4 ± 1.0	<1.1	<3.4	15.18[a]	∼1.1[b]	60[c]	O8 V or B0 III	0.5[d] (0.1–2; *R*) 1.3 (0.16–3.5; *E*) 8–11[d,e] (0.2–10; *X*) <0.027 (0.2–10; *N*) 15–30 (0.3–10; *X*)
RX J0101.8−7223	28.4 ± 1.4	46 ± 2	2.4 ± 0.5	10 ± 2	∼14.8[f]	∼1.5	60[c]	O9–B0 III	2.3–5.8[g] (0.2–10; *A*, *R*, *N*) 3.9[f] (0.2–10; *N*) 36.5[h] (0.2–10; *N*)
IGR J22534+6243	31.8 ± 1.6	81.0 ± 0.4	3.4 ± 0.5	3.3 ± 0.5	13.7	∼6.7	∼4.4	early B III	0.003 (0.1–2.4; *R*) 0.012–0.10 (0.5–10; *R*, *X*, *C*) 0.14 (17–60; *I*)
IGR J18256−1035	5.5 ± 0.5	0.11 ± 0.03	<10	<0.03	—	—	8[i]	—	0.22 (0.3–10; *C*) 0.15 (2–10; *X*) 0.47 (20–40; *I*) <0.21 (40–100; *I*) 0.56 (17–60; *I*)

Notes. The upper part of the table deals with the HMXBs identified here, whereas the lower part reports on the single LMXB of our sample. EWs are expressed in Å, line fluxes are in units of 10^{-15} erg cm^{-2} s^{-1}, X-ray luminosities are in units of 10^{35} erg s^{-1}, and the reference band (between round brackets) is expressed in keV. In the last column, the upper case letter indicates the satellite and/or the instrument with which the corresponding X-ray flux measurement was obtained (see text). [(a)] from Massey (2002); [(b)] only the Galactic reddening along the line of sight was assumed; [(c)] from Harries et al. (2003); [(d)] from Coe et al. (2010); [(e)] from Sturm et al. 2011; [(f)] from Haberl et al. (2008); [(g)] from Haberl & Pietsch (2004); [(h)] from Townsend et al. (2013); [(i)] assumed (see text).

Table 8. Synoptic table containing the main results concerning the five CVs identified in the present sample of INTEGRAL sources (see Fig. 11).

Object	H_α		H_β		He II λ4686		R	A_V	d	L_X
	EW	Flux	*EW*	Flux	*EW*	Flux	mag	(mag)	(pc)	
Swift J0958.0−4208	30.6 ± 1.5	34.6 ± 1.7	16.1 ± 0.8	21.6 ± 1.1	19.6 ± 1.0	26.5 ± 1.3	15.5[a]	∼0	∼200	2.2 (2–10; *X*) 6.7 (17–60; *I*) 4.0 (15–150; *B*) 4.4 (14–195; *B*)
IGR J14257−6117	75 ± 5	8.4 ± 0.6	18 ± 3	1.4 ± 0.2	16 ± 2	1.19 ± 0.18	17.2	∼2.3	1000[b]	53 (2–10; *X*) 87 (17–60; *I*) 130 (14–195; *B*)
IGR J17014−4306	11.1 ± 0.6	16.4 ± 0.8	13.2 ± 1.3	16.1 ± 1.6	10.4 ± 1.6	11.9 ± 1.8	15.1	∼0	∼170	0.90 (0.2–12; *N*) 2.5 (17–60; *I*) 3.0 (15–150; *B*) 5.5 (14–195; *B*)
IGR J18151−1052	29 ± 2	0.89 ± 0.06	12 ± 4	0.10 ± 0.03	<10	<0.08	≈18[c]	∼3.6	1000[b]	48 (2–10; *X*) 110 (17–60; *I*) 110 (15–150; *B*)
AX J1832.3−0840	50 ± 5	1.50 ± 0.15	43 ± 9	0.37 ± 0.07	36 ± 12	0.15 ± 0.05	19.6[c]	∼1.1	1000[b]	110 (0.2–12; *N*) 130 (0.7–10; *A*) 84 (2–10; *N*) 74 (17–60; *I*) 45 (20–100; *I*)

Notes. EWs are expressed in Å, line fluxes are in units of 10^{-15} erg cm^{-2} s^{-1}, X-ray luminosities are in units of 10^{31} erg s^{-1}, and the reference band (between round brackets) is expressed in keV. In the last column, the upper case letter indicates the satellite and/or the instrument with which the corresponding X-ray flux measurement was obtained (see text). [(a)] from Monet et al. (2003); [(b)] assumed (see text); [(c)] from Lutovinov et al. (2012).

Table 9. Main observational results for the active star IGR J17198−3020 (see Fig. 12) as identified in the present sample of INTEGRAL sources.

Object	H_α		R	A_V	d	L_X
	EW	Flux	mag	(mag)	(pc)	
IGR J17198−3020	1.02 ± 0.15	6.3 ± 0.9	12.3	∼0.9	∼350	0.83 (0.3–10; *X*) 10 (20–100; *I*)

Notes. EWs are expressed in Å, line fluxes are in units of 10^{-15} erg cm^{-2} s^{-1}, X-ray luminosities are in units of 10^{31} erg s^{-1}, and the reference band (between round brackets) is expressed in keV. In the last column, the upper case letter indicates the satellite and/or the instrument with which the corresponding X-ray flux measurement was obtained (see text).

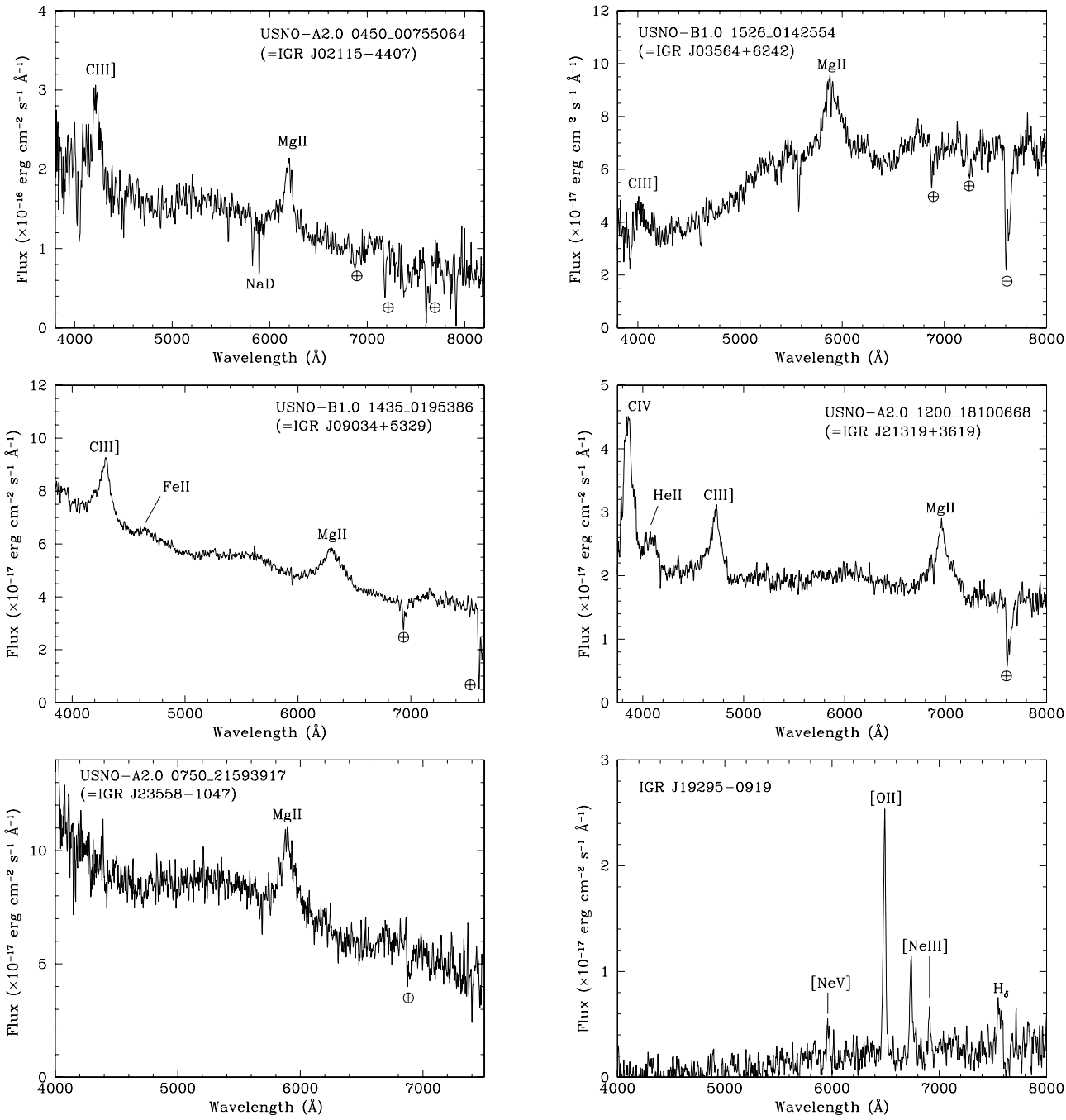

Fig. 5. Spectra (not corrected for the intervening Galactic absorption) of the optical counterparts of the six high-redshift QSOs presented in this paper for the first time. For each spectrum, the main spectral features are labelled. The symbol ⊕ indicates atmospheric telluric absorption bands. The TNG and SPM spectra have been smoothed using a Gaussian filter with $\sigma = 3$ Å. The spectrum of the only Type 2 QSO present in this sample (IGR J19295−0919) is reported in the *lower right panel* of the figure.

of the measured 2–10 keV X-ray flux to the unabsorbed flux of the [O III]λ5007 forbidden emission line. This approach allows us to infer their Compton nature. We find that the value of T is 3.4, 14.1, and 0.57 for LEDA 7910, LEDA 2287192, and LEDA 3077397, respectively, after correction of the [O III]λ5007 emission line flux for the absorption local to the corresponding AGN (see Table 5). This points to a Compton thick source classification for the latter AGN, whereas the two other cases lie in the Compton thin regime. We stress that the above values should actually be considered as upper limits for T because the soft X-ray fluxes that we used refer to bands which are wider than the ones for which this method should be applied (see Table 5).

Actually, this latter result is at variance with the findings of Tomsick et al. (2012), who did not detect any absorption local to the AGN for LEDA 3077397. A possible way out to this discrepancy lies in the evidence (e.g., Trippe et al. 2011) that Compton thick AGNs may fictitiously display no appreciable X-ray absorption with a flat X-ray spectrum. This is due to the large actual $N_{\rm H}$, which suppresses the direct continuum below 10 keV, so that only the reflected component is observed in this energy range with a spectrum characterized by a photon index $\Gamma < 0.5$ (as indeed observed from LEDA 3077397 by Tomsick et al. 2012).

Finally, we applied the following prescriptions to infer the mass of the central black hole in the broad-line AGNs of our

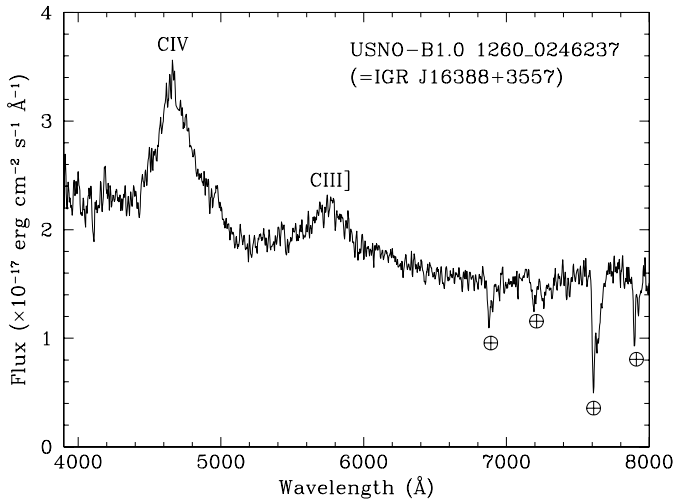

Fig. 6. Spectrum (not corrected for the intervening Galactic absorption) of the Type 1 QSO IGR J16388+3557 with the correct emission line identifications, which allow us to determine a redshift $z = 2.020 \pm 0.005$ for the source. The symbol $\oplus$ indicates atmospheric telluric absorption bands. The spectrum has been smoothed using a Gaussian filter with $\sigma = 3$ Å.

sample. The choice of the method varies according to the spectral emission line used for the estimate. For the cases in which the H_β emission is within the covered optical spectral range, we used the approach of Wu et al. (2004) and Kaspi et al. (2000). Otherwise, we apply the formulae from McLure & Jarvis (2002) or Assef et al. (2011), which use the information afforded by the Mg II or C IV broad emissions, respectively. In this way we were able to compute an estimate of the mass of the central black hole for all 13 broad-line AGNs presented in this paper for the first time plus the correct value for IGR J16388+3557 (see Table 6). In all cases, we assumed a null local absorption.

As already remarked in Paper IX, the main sources of error in these mass estimates generally come from the determination of the flux of the employed emission lines, which is around 15% in the present sample (see Tables 3 and 4), and from the scatter in the scaling relation between the size of the BLR and the diagnostic line luminosity (Vestergaard 2004). As a whole, we expect the typical error to be about 50% of the black hole mass value.

In Table 6, we also list the apparent Eddington ratios for these AGNs. These were computed using the observed X-ray fluxes and/or upper limits in the 20–100 keV band. When needed, we rescaled the observed luminosities to the above spectral range assuming a photon index $\Gamma = 1.8$.

Even considering all the above caveats and making the same considerations as in Paper IX, we see that the values of the Eddington ratios in Table 6 suggest a very energetic nature for several Type 1 AGNs of our sample, especially those at high redshift, which is in line with cases already found in hard X-ray surveys (see e.g. Lanzuisi et al. 2012; Bassani et al. 2012). This supports the scenario of Ghisellini et al. (2011), according to which many powerful blazars emit most of their energy in the MeV band or below, and implies that these objects are more efficiently searched in hard X-rays rather than in the GeV range.

4.2. X-ray binaries

Among the other objects identified in our sample of INTEGRAL sources in this paper we found four cases, which could be classified as X-ray binaries. Three of them show the characteristics of HMXBs – two are located in the Small Magellanic Cloud (SMC) and one in the Galaxy – while one is classified as a generic X-ray binary but is probably a low-mass one (LMXB; see below).

The objects IGR J00515−7328, RX J0101.8−7223, and IGR J22534+6243 are identified as HMXBs due to the presence of an H_α emission at a redshift consistent with 0 superimposed on an intrinsically blue spectral continuum; in the latter two cases, He I and/or H_β emission lines are also detected (see Fig. 10 and Table 7). We however note that the spectral shape of IGR J22534+6243 appears to be substantially modified by intervening reddening. This points to the presence of interstellar dust along the source line of sight. This result is indeed usual for Galactic HMXBs detected with INTEGRAL (e.g., Papers III–IX) and indicates that the object lies far from the Earth.

The HMXB identification for RX J0101.8−7223 and IGR J22534+6243 is also independently supported by the detection of X-ray pulsations (Townsend et al. 2013; Esposito et al. 2013), strongly pointing to the presence of an accreting neutron star hosted in these systems.

Concerning IGR J18256−1035, an H_α emission found again at redshift 0 is detected on a red spectral continuum. The faintness of the optical counterpart along with the optical spectral shape and the NIR non-detection in the 2MASS catalogue (Skrutskie et al. 2006) does not favor the presence of an early type companion and, consequently, a classification as HMXB. Given the relative faintness of the H_α emission line with respect to that detected in similarly reddened CVs (see Paper IX and Sect. 4.3), we suggest to classify this source as a LMXB.

For all these objects, Table 7 lists the relevant optical spectral information along with the main parametres determined from the available X-ray and optical data. When not indicated otherwise, X-ray luminosities in Table 7 were calculated using the fluxes extracted from Wang & Wu (1992), Voges et al. (2000), Landi et al. (2007, 2013), Tomsick et al. (2008), Bird et al. (2010), Kennea (2011), Sturm et al. (2011), Krivonos et al. (2012), and Esposito et al. (2013). Constraints on distance, reddening, spectral type, and X-ray luminosity shown in Table 7 for the identified HMXBs were derived by considering the absolute magnitudes of early-type stars and by applying the method described in Papers III and IV for the classification of this type of X-ray sources.

Regarding the determination of the distance for the X-ray binaries discussed in this section, we assumed that IGR J00515−7328 and RX J0101.8−7223 are located in the SMC and thus at a distance of 60 kpc (Harries et al. 2003), whereas a distance of 8 kpc was assumed for IGR J18256−1035; no inferences on this value were otherwise possible due to the lack of sufficient optical/NIR information on its counterpart. For IGR J22534+6243, we exclude the possibility that its companion is of luminosity class I because it would lie outside the Galactic disk (>8 kpc from Earth) according to the map of Leicht & Vasisht (1998). Likewise, the presence of substantial reddening towards this source would place the source in or beyond the Perseus Arm of the Galaxy, suggesting a distance >3 kpc. This figure is also too large to support a luminosity class V for the optical companion. This analysis indicates that all HMXBs identified here most likely belong to the subclass of Be/X binaries.

Considering the equivalent widths (EWs) of the H_α emission of the three HMXBs in our sample and following the empirical relation of Antoniou et al. (2009) that connects this observable with the orbital period of Be/X binaries, we infer that RX J0101.8−7223 and IGR J22534+6243 may have

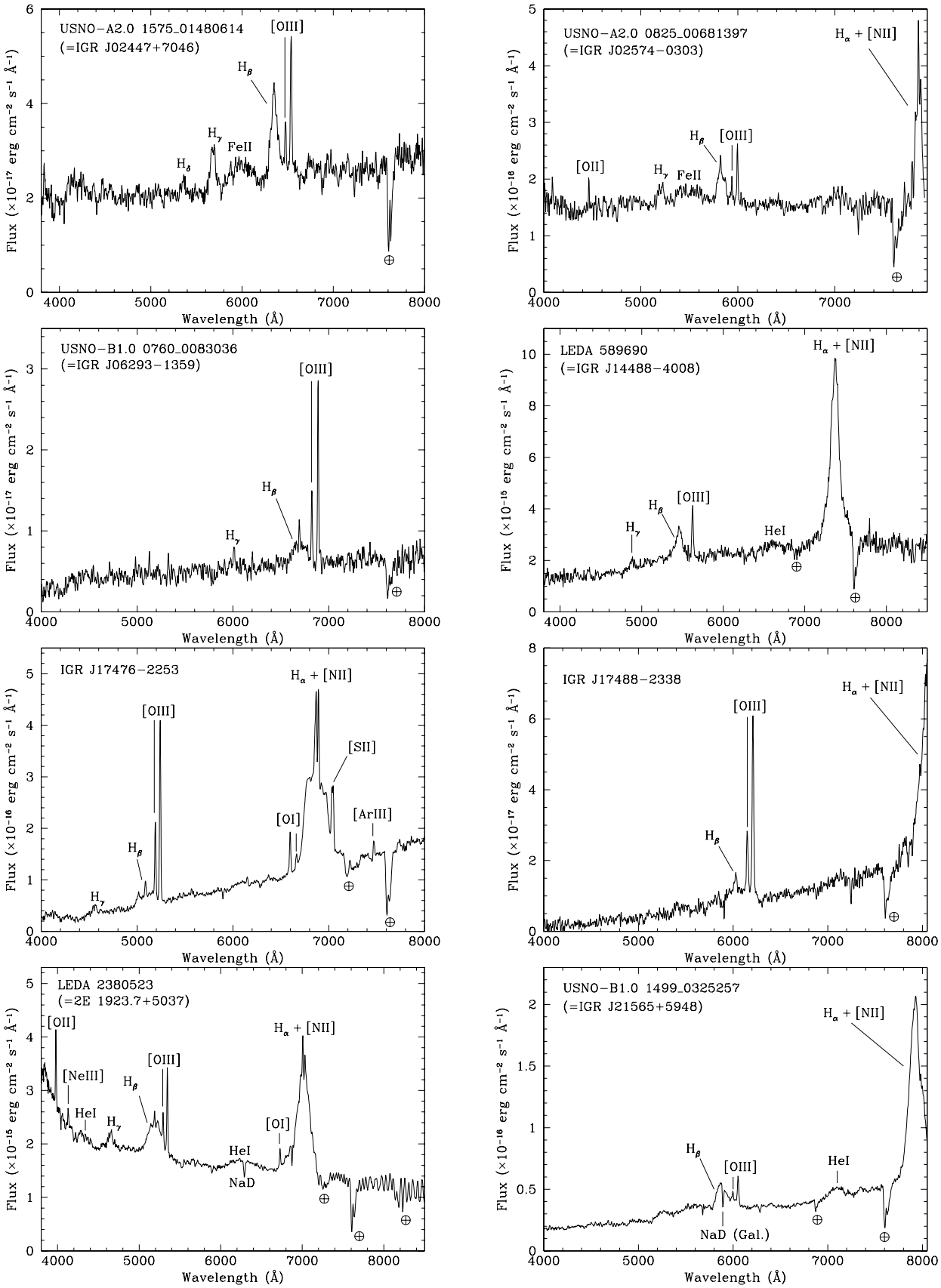

Fig. 7. Spectra (not corrected for the intervening Galactic absorption) of the optical counterparts of the eight low-redshift, broad emission-line AGNs belonging to the sample of INTEGRAL sources presented in this paper. For each spectrum, the main spectral features are labelled. The symbol ⊕ indicates atmospheric telluric absorption bands. The TNG spectra have been smoothed using a Gaussian filter with $\sigma = 3$ Å.

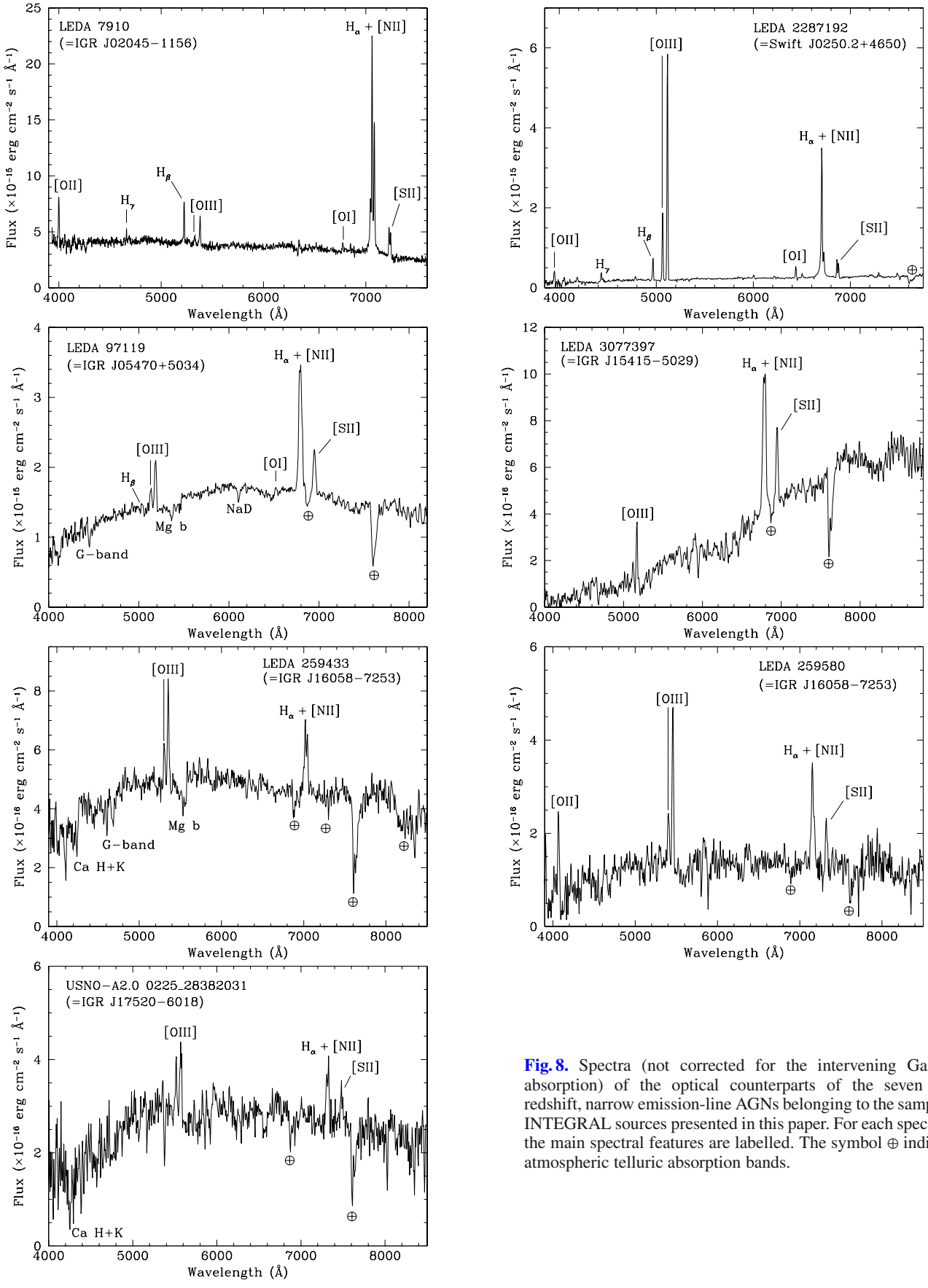

Fig. 8. Spectra (not corrected for the intervening Galactic absorption) of the optical counterparts of the seven low-redshift, narrow emission-line AGNs belonging to the sample of INTEGRAL sources presented in this paper. For each spectrum, the main spectral features are labelled. The symbol ⊕ indicates atmospheric telluric absorption bands.

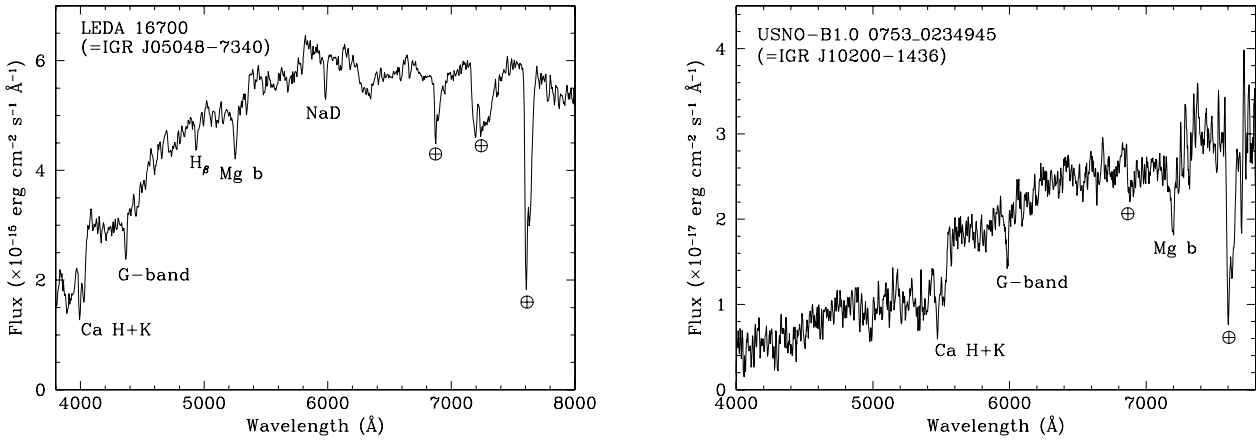

Fig. 9. Spectra (not corrected for the intervening Galactic absorption) of the optical counterparts of the two XBONGs belonging to the sample of INTEGRAL sources presented in this paper. For each spectrum, the main spectral features are labelled. The symbol ⊕ indicates atmospheric telluric absorption bands. The spectrum of IGR J10200−1436 has been smoothed using a Gaussian filter with σ = 3 Å.

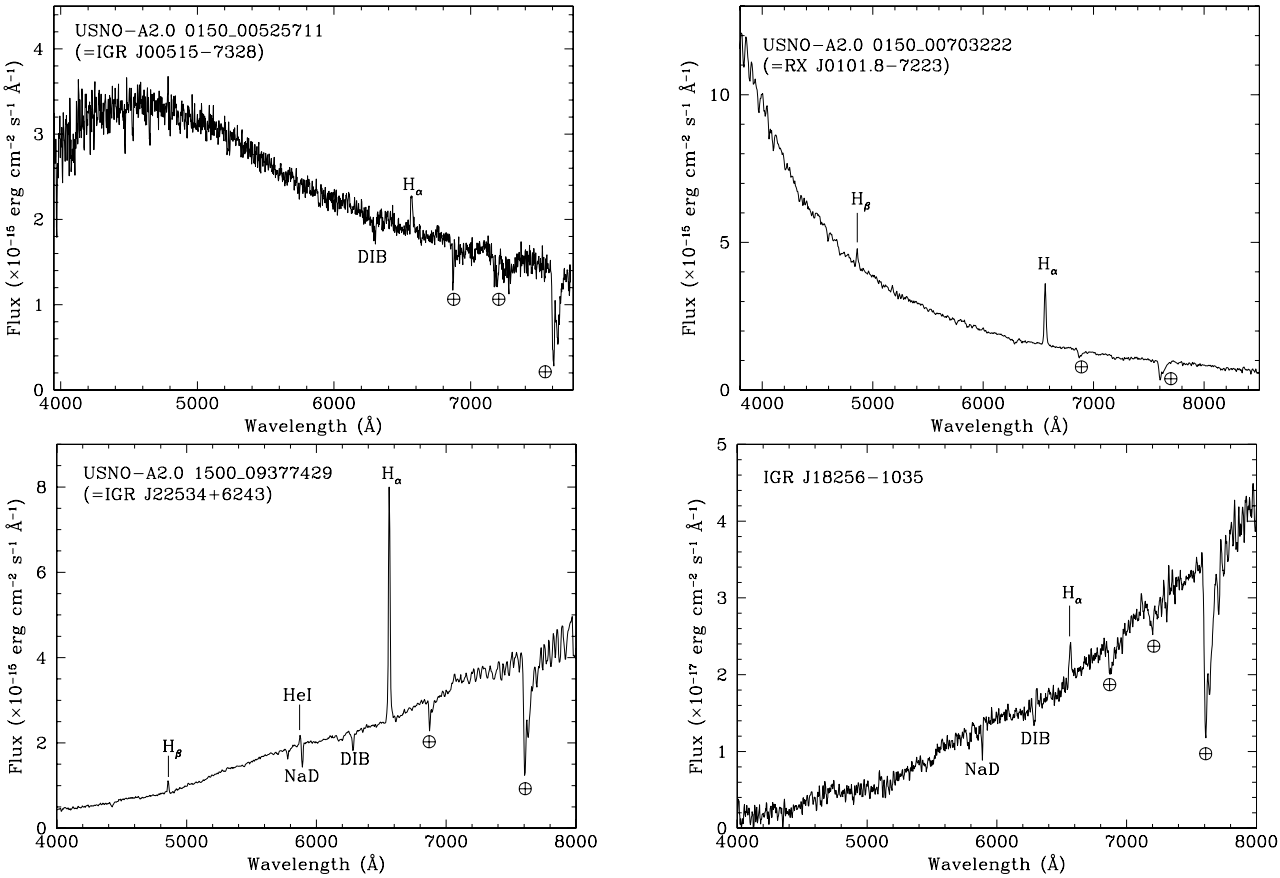

Fig. 10. Spectra (not corrected for the intervening Galactic absorption) of the optical counterparts of the four X-ray binaries belonging to the sample of INTEGRAL sources presented in this paper. For each spectrum, the main spectral features are labelled. The symbol ⊕ indicates atmospheric telluric absorption bands.

$P_{\rm orb} \approx 100$ d, whereas this value is $\lesssim$20 d for IGR J00515−7328. For RX J0101.8−7223, this suggestion is confirmed by the periodicity analysis of the optical light curve by Townsend et al. (2013).

It should be stressed that our optical results are broadly consistent with those of Townsend et al. (2013) and Esposito et al. (2013), which presented optical spectra of the counterparts of RX J0101.8−7223 and IGR J22534+6243, respectively, with resolution higher than ours. For the other cases, detailed photometric optical/NIR information and higher-resolution spectroscopy is mandatory to refine the spectral classification and properties of these objects.

To conclude this section, we mention that none of these objects has any known radio source positionally associated with

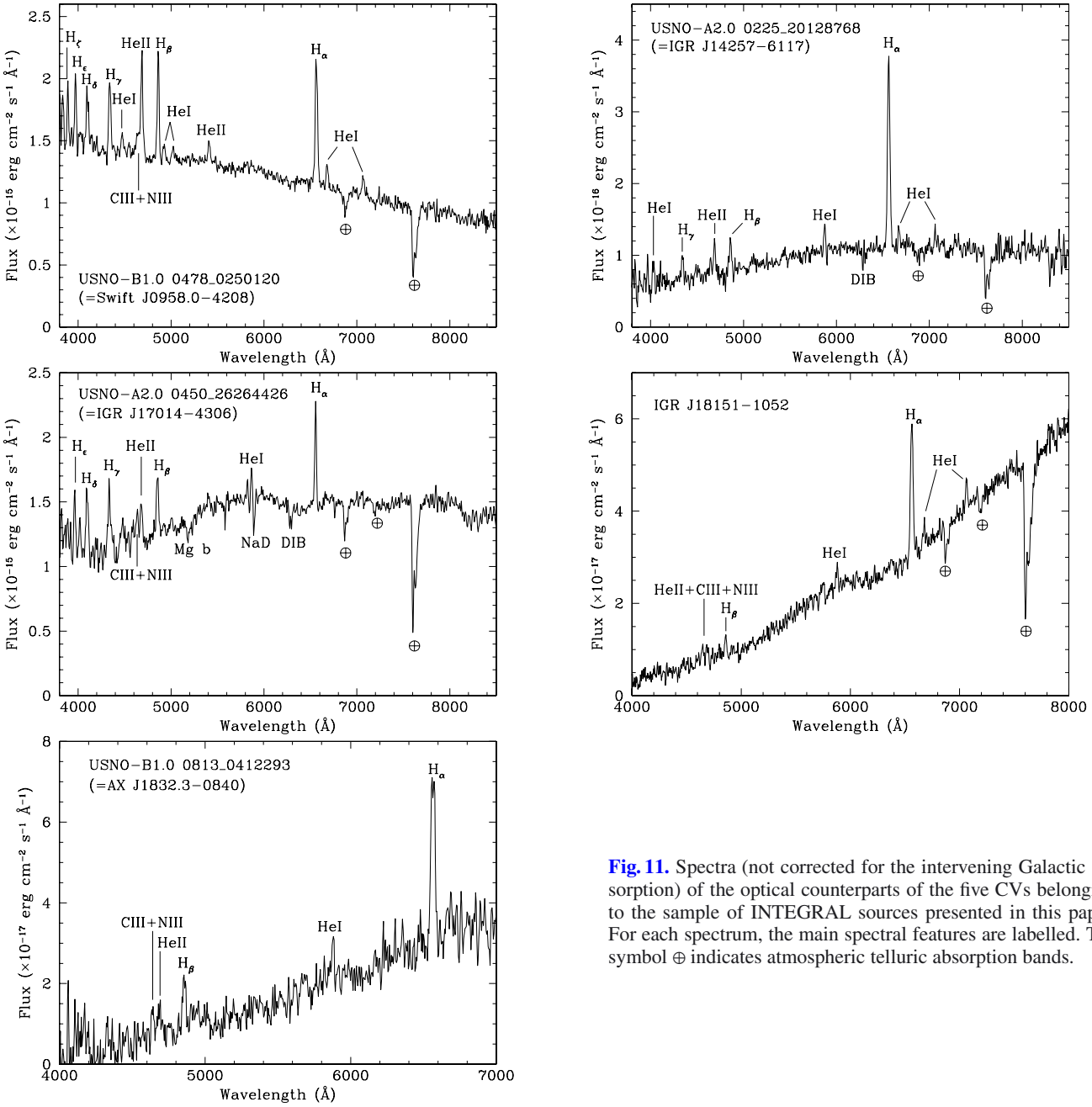

Fig. 11. Spectra (not corrected for the intervening Galactic absorption) of the optical counterparts of the five CVs belonging to the sample of INTEGRAL sources presented in this paper. For each spectrum, the main spectral features are labelled. The symbol ⊕ indicates atmospheric telluric absorption bands.

them. This indicates that all these X-ray binaries are unlikely to produce collimated (jet-like) outflows; that is, their microquasar nature can be ruled out.

4.3. CVs

Spectroscopy of the five sources classified as CVs in our present sample (Fig. 11) indicates the typical characteristics of objects belonging to this class – that is, Balmer (up to H_ζ for the optical counterpart of Swift J0958.0−4208) and helium emission lines. In all cases these spectral features are at redshift $z = 0$, which of course means that these objects lie within the Galaxy. Our spectroscopic results for IGR J18151−1052 are consistent with those reported by Lutovinov et al. (2012) for this source.

The main spectroscopic results and the main astrophysical parametres, which can be inferred from the available observational data, are reported in Table 8. The X-ray luminosities in this table were obtained using the fluxes of Sugizaki et al. (2000), Watson et al. (2009), Cusumano et al. (2010), Kaur et al. (2010), Scaringi et al. (2010), Krivonos et al. (2010, 2012), Landi et al. (2012a, 2013), Lutovinov et al. (2012), and Baumgartner et al. (2013).

It can be noted from Table 8 that Swift J0958.0−4208 shows an He II λ4686/H_β equivalent width (EW) ratio that is larger than 1; moreover, this same parametre approaches unity in sources IGR J14257−6117, IGR J17014−4306 and AX J1832.3−0840. Besides, in nearly all CVs of our sample the EWs of these two emission lines are larger than 10 Å. This strongly indicates that these sources are possibly harboring a magnetized white dwarf (WD) and thus may be polar or intermediate polar (IP) CVs (see e.g. Cropper 1990 and Warner 1995). This further supports the IP CV classification suggested for AX J1832.3−0840 from the X-ray data analysis (Kaur et al. 2010, and references therein).

We however recall that this proposed classification for the other four sources needs an independent confirmation through the measurement of both the orbital and the WD spin periods, given that optical spectroscopy alone is sometimes insufficient to determine the magnetic nature of CVs (see e.g. Pretorius 2009; and de Martino et al. 2010).

It should be noted that three of these objects with the exception of Swift J0958.0−4208 and IGR J17014−4306 show the presence of reddening along the line of sight. This can be stated from the continuum shape and the H_α/H_β flux ratio. Using this parametre we estimate the value for the absorption in the optical V band along the line of sight to these sources (reported in Table 8). Because of the uncertainties tied to the distance determination for absorbed CVs (see e.g. Paper IX), we do not attempt such an evaluation and we assume a distance of 1 kpc for these objects. For these three cases we also note that the V-band absorption inferred from the Balmer line ratio is always (and, in some cases, remarkably) lower than the Galactic one along their direction (that is, ∼33, ∼4.4, and ∼60 mag for IGR J14257−6117, IGR J18151−1052, and AX J1832.3−0840, respectively, according to Schlegel et al. 1998). This suggests that they are located in the near side of the Galaxy.

We conclude this section by recalling that two soft X-ray sources (#1 and #2 in Landi et al. 2013) are found within the hard X-ray error circle of Swift J0958.0−4208 with the stronger one (#1) positionally associated with the CV identified in this work. If we follow the prescription of Tomsick et al. (2012), consider the X-ray fluxes reported in Landi et al. (2013), and use the conservative error radius of Baumgartner et al. (2013) for Swift J0958.0−4208, we find that the positional chance coincidence probabilities for sources #1 and #2 of Landi et al. (2013) of being associated with this hard X-ray object are 1% and 9%, respectively. This result suggests that, indeed, the CV identified here has the largest probability of being physically associated with Swift J0958.0−4208; however, we cannot exclude a contribution from the other object (#2) to the total high-energy flux of this source detected with INTEGRAL. More observations are thus needed to clarify this issue and the nature of source #2 of Landi et al. (2013).

4.4. Active stars

As seen in Fig. 12, the optical counterpart of source IGR J17198−3020 shows a star-like continuum typical of late-G/early-K type stars with a faint but nevertheless evident H_α emission at $z = 0$. This is comparable to what was found in other cases that were tentatively identified as RS CVn stars (Paper VI; Paper IX). We thus suggest that this source can be classified as a chromospherically active star as well. This conclusion is also supported by the apparent X-ray variability pointed out for this object by Bird et al. (2010; see also Sect. 2).

The main observed and inferred parametres for this object are listed in Table 9. Luminosities are computed using the X-ray fluxes given in Bird et al. (2010) and Luna et al. (2012).

Assuming a similarity with the active star II Peg (with magnitude $R \sim 6.9$ and distance 40 pc; see Monet et al. 2003; van Leeuwen 2007 and Paper IX) as suggested in Rodriguez et al. (2010), we obtain a distance of 480 pc for IGR J17198−3020. However, this figure should strictly be considered as an upper limit, given that no correction for the interstellar absorption was applied. This should actually be present, due to the reddened appearance of the optical spectrum of this object when compared to similar sources in Papers VI and IX. If we correct the $B - R$ color index (2.9 mag) of the optical counterpart of IGR J17198−3020 so to bring it equal to the one of II Peg (1.5 mag; Monet et al. 2003), we derive an absorption $A_V \sim 0.9$ mag and in turn a distance $d \sim 350$ pc for the source. An independent support to this approach comes from the fact that this value for A_V is compatible with the hydrogen column density N_H derived by Luna et al. (2012), if we assume the empirical formula of Predehl & Schmitt (1995). We thus used this latter value for the distance to determine the X-ray luminosities reported in Table 9. Clearly, a deeper multiwavelength follow-up is vividly advised to better characterize this active star identification also in this case.

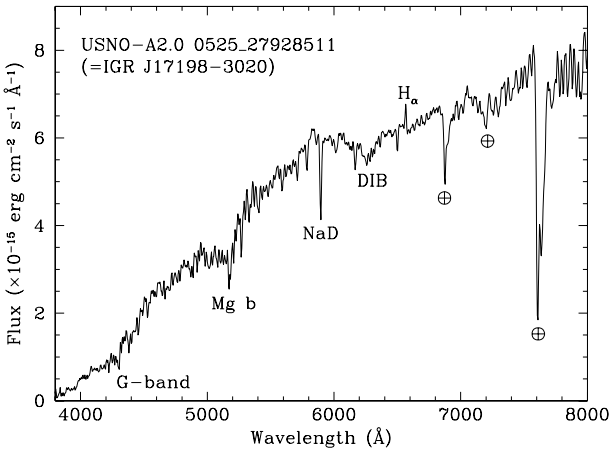

Fig. 12. Spectrum (not corrected for the intervening Galactic absorption) of the optical counterpart of the chromospherically active star IGR J17198−3020 belonging to the sample of INTEGRAL sources presented in this paper. The main spectral features are labelled. The symbol ⊕ indicates atmospheric telluric absorption bands.

4.5. Statistics

As done in our previous papers, we give an update of the statistics concerning the identifications of new hard X-ray INTEGRAL sources including the results of this work and those in Lutovinov et al. (2012), Smith et al. (2012), Sturm et al. (2012), and Ratti et al. (2013). Up to now, 240 INTEGRAL objects have been identified through optical or NIR spectroscopy; their separation into the main classes reported in Papers VI-IX is the following: 147 (61.2%) are AGNs, 60 (25.0%) are X-ray binaries, 29 (12.1%) are CVs, and 4 cases (1.7%) are likely identified as active stars. This seems to confirm a possible observational bias towards the former group of sources (see the discussion in Papers VIII and IX). We also keep detecting (likely magnetic) CVs within the considered putative counterparts of hard X-ray sources.

By examining the breakdown of low-redshift ($z < 0.5$) AGN subclasses, we see that 68 objects (that is, 55% of the AGN identifications) are Seyfert 1 galaxies and 54 (44%) are narrow-line AGNs (including 50 Seyfert 2 galaxies and 4 LINERs), while the high-redshift ($z > 0.5$) QSOs, the XBONGs, and the BL Lacs amount to 16, 6, and 3 objects (7%, 2%, and 1% of the total of identified INTEGRAL sources), respectively.

It is moreover confirmed that a substantial number of high-redshift QSOs can be found with the use of medium-sized telescopes (such as TNG in the present study). With this paper, we increase the number of newly-identified INTEGRAL sources at $z > 0.5$ by more than 50% (that is, from 10 to 16), allowing a deeper mapping of the distribution and properties of these high-z, high-energy sources.

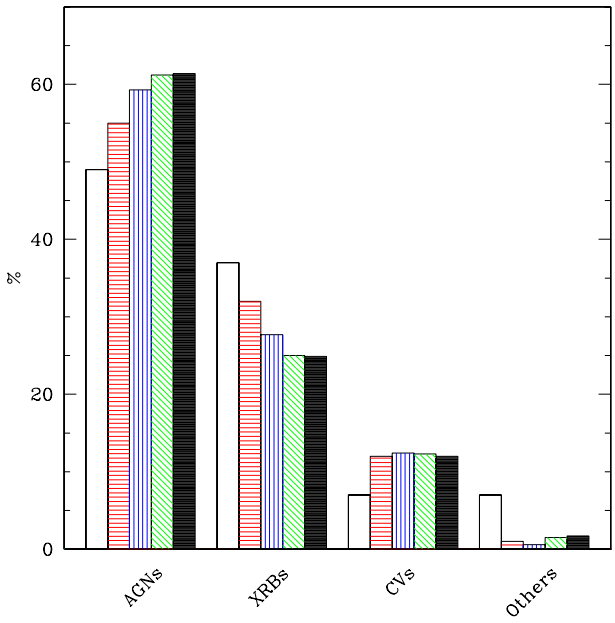

Fig. 13. Histogram, subdivided into source types, showing the percentage of INTEGRAL objects of known nature in the fourth IBIS survey (Bird et al. 2010; open columns) and of INTEGRAL sources from various surveys and identified through optical or NIR spectroscopy at the time of acceptance of papers VII (November 2008; horizontally dashed columns), VIII (May 2010; vertically dashed columns), and IX (December 2011; diagonally dashed columns) along with those in the present one (filled columns).

When we compare the average AGN redshift of the known extragalactic sources in the IBIS surveys ($\langle z \rangle \sim 0.14$: Bird et al. 2010; Krivonos et al. 2010, 2012) to that of the sample of the present paper ($\langle z \rangle = 0.404$), we see that this value, albeit slightly lower than that of the sample in Paper IX, corroborates the results of that work. In particular, it indicates on average that we can explore the hard X-ray sky at distances that are more than three times larger than those of the known emitting sources belonging to the INTEGRAL surveys. Moreover, nearly half (11 out of 23) of the AGNs identified here lie farther than the above mentioned average redshift of known catalogued IBIS objects. We also remark that a non-negligible contribution to this search is afforded by 2-metre class telescopes, as two of the six high-z QSOs of our sample have been identified with this type of facility.

We also find that the large majority of the high-redshift QSOs found in our identification program are of Type 1 (the only Type 2 case being IGR J19295−0919, as reported in Sect. 4.1). This is reasonably explained by the evidence that soft X-rays, needed for a precise localization of the source, are not easily detected from Type 2 QSOs due to local absorption in these sources, which adds to the faintness tied to their distance.

Concerning the Galactic objects, we find that 45 and 14 objects (i.e. 75% and 23% of the X-ray binary identifications) are HMXBs and LMXBs, respectively, whereas a single one is classified as an intermediate-mass X-ray binary (see Ratti et al. 2013). In addition, most of the sources hosting an accreting WD (24, that is 83% of them) are definite or likely dwarf novae (eminently of magnetic type), and the remaining 5 are symbiotic stars.

A comparison of the above figures with those in the largest INTEGRAL survey of Bird et al. (2010) and those of our previous Papers VII–IX (see the histograms in Fig. 13) indicates no significant changes in the relative weights among the various classes; rather, a saturation of the identification percentages seems to have been reached. Finally, we remark that 206 of the 240 optical and NIR spectroscopic identifications examined in this section (i.e., more than 85% of the total) were obtained within the framework of our spectroscopic follow-up program originally started in 2004 (Papers I-IX, the present work, and references therein).

5. Conclusions

We presented further results from our ongoing identification program of INTEGRAL sources through optical spectroscopy (Papers I-IX) at various telescopes worldwide. In the present work, we identified and characterized 33 objects (two of which contribute to the hard X-ray emission labelled as source IGR J16058−7253) with an unknown or poorly explored nature, which are listed in hard X-ray sky surveys from this satellite. This was accomplished with the use of six telescopes of different apertures from 1.5 to 3.6 metres and of archival data from one spectroscopic survey.

Our main results are as follows.

- The majority of identifications is made of AGNs. Most of them (13) are of Type 1, eight cases are of Type 2, and two are XBONGs. This confirms the trend of our previous findings that optical spectroscopy preferentially allows the identification of hard X-ray emitting AGNs.
- Six of these AGNs lie at high redshift ($z > 0.5$), and five lie at $z > 1$. This allowed the detections of high-z, high-energy emitting QSOs to increase by 50%. We also show that the black hole mass estimates for these sources support the idea that hard X-ray surveys may efficiently identify powerful AGNs in the distant Universe.
- The only LINER found in the present sample, IGR J02045−1156, had an intermediate Seyfert 1 appearance in an optical spectrum acquired in the late 1980s. This indicates that a change in the AGN environment structure occurred for this source.
- Ten objects lie in the local Universe, eight in the Galaxy, and two in the SMC. Of them, five are CVs, three are Be/X HMXBs (two of them belong to the SMC), one is a LMXB, and one is possibly a flare star of RS CVn type. This finding again supports that a non-negligible percentage of hard X-ray CVs is routinely found in optical spectroscopic searches for unidentified high-energy sources.

We also report to the best of our knowledge the discovery of the farthest hard X-ray emitting XBONG (IGR J10200−1436, at $z = 0.391$) and of the farthest Type 2 QSO (IGR J19295−0919, at $z = 0.741$) within the INTEGRAL surveys. This confirms the importance of this identification work on catalogued but unidentified high-energy sources, because peculiar objects can be found within the considered samples (see, for instance, Paper IX; Masetti et al. 2007, 2008b; Bassani et al. 2012; de Martino et al. 2010, 2013). With the present data, we also correct two results given in Paper IX, namely the actual redshift ($z = 2.02$) of the Type 1 QSO IGR J16388+3557 and the correct counterpart of source IGR J06293−1359. We again stress that our findings indicate the validity of this approach, which combines X-ray catalogue cross-correlation, follow-up observations with soft X-ray satellites capable of providing arcsec-sized error boxes (such as *Chandra*, *XMM-Newton*, *Swift* or *NuSTAR*), and optical spectroscopy to pinpoint the nature of still unidentified or poorly known INTEGRAL sources.

Present and future surveys at optical and NIR wavelengths, such as the ongoing Vista Variables in the Vía Láctea (VVV: Minniti et al. 2010; Saito et al. 2012) public NIR survey, will permit the identification of variable sources in the fields of the objects detected in published and forthcoming INTEGRAL catalogues. This will facilitate the detection of putative NIR counterparts for these high-energy sources by means of accurate positional information and/or variability studies. This approach was already tested, providing encouraging results and allowing constraints on the nature of transient and persistent hard X-ray sources, especially in crowded fields such as those along the Galactic plane and bulge (Rojas et al. 2012a,b, 2013; and in prep.).

Acknowledgements. We thank Silvia Galleti for Service Mode observations at the Loiano telescope, and Roberto Gualandi for night assistance; Giorgio Martorana and Mauro Rebeschini for Service Mode observations at the Asiago telescope and Luciano Traverso for coordinating them; Aldo Fiorenzano, Vania Lorenzi and Walter Boschin for Service Mode observations at the TNG; Manuel Hernández, Rodrigo Hernández, Alberto Álvarez and Alberto Miranda for Service Mode observations at the CTIO telescope and Fred Walter for coordinating them. NM thanks Daniel Stern for useful discussions. We also thank the anonymous referee for the high consideration expressed about this work. This research has made use of the ASI Science Data Center Multimission Archive; it also used the NASA Astrophysics Data System Abstract Service, the NASA/IPAC Extragalactic Database (NED), and the NASA/IPAC Infrared Science Archive, which are operated by the Jet Propulsion Laboratory, California Institute of Technology, under contract with the National Aeronautics and Space Administration. This publication made use of data products from the Two Micron All Sky Survey (2MASS), which is a joint project of the University of Massachusetts and the Infrared Processing and Analysis Center/California Institute of Technology, funded by the National Aeronautics and Space Administration and the National Science Foundation. This research has also made use of data extracted from the Six-degree Field Galaxy Survey archive; it has also made use of the SIMBAD and VIZIER databases operated at CDS, Strasbourg, France, and of the HyperLeda catalogue operated at the Observatoire de Lyon, France. NM acknowledges financial support via ASI-INAF agreement No. I/009/10/0 and thanks the Departamento de Astronomía y Astrofísica of the Pontificia Universidad Católica de Chile in Santiago for the warm hospitality during the preparation of this paper. PP and RL are supported by the ASI-INAF agreement No. I/033/10/0. DM is supported by the BASAL CATA PFB-06 and FONDECYT No. 1130196 grants. LM acknowledges financial support from the University of Padua through grant No. CPS0204.

References

Antoniou, V., Hatzidimitriou, D., Zezas, A., & Reig, P. 2009, ApJ, 707, 1080
Assafin, M., Andrei, A. H., Vieira Martins, R., et al. 2001, ApJ, 552, 380
Assef, R. J., Denney, K. D., Kochanek, C. S., et al. 2011, ApJ, 742, 93
Augarde, R., Chalabaev, A., Comte, G., Kunth, D., & Maehara, H. 1994, A&AS, 104, 259
Bassani, L., Dadina, M., Maiolino, R., et al. 1999, ApJS, 121, 473
Bassani, L., Landi, R., Marshall, F. E., et al. 2012, A&A, 543, A1
Baumgartner, W. H., Tueller, J., Markwardt, C. B., et al. 2013, ApJS, 207, 19
Bikmaev, I., Irtuganov, E., Sakhibullin, N., et al. 2010, ATel #3072
Bird, A. J., Bazzano, A., Bassani, L., et al. 2010, ApJS, 186, 1
Bottacini, E., Ajello, M., & Greiner, J. 2012, ApJS, 201, 34
Cardelli, J. A., Clayton, G. C., & Mathis, J. S. 1989, ApJ, 345, 245
Coe, M. J., Bird, A. J., Buckley, D. A. H., et al. 2010, MNRAS, 406, 2533
Comastri, A., Mignoli, M., Ciliegi, P., et al. 2002, ApJ, 571, 771
Condon, J. J., Cotton, W. D., Greisen, E. W., et al. 1998, AJ, 115, 1693
Cropper, M. 1990, Space Sci. Rev., 54, 195
Cusumano, G., La Parola, V., Segreto, A., et al. 2010, A&A, 524, A64
David, L. P., Jones, C., & Forman, W. 1992, ApJ, 388, 82
de Martino, D., Falanga, M., Bonnet-Bidaud, J.-M., et al. 2010, A&A, 515, A25
de Martino, D., Belloni, T., Falanga, M., et al. 2013, A&A, 550, A89
Del Santo, M., Sidoli, L., Mereghetti, S., et al. 2007, A&A, 468, L17
Deutsch, E. W. 1999, AJ, 118, 1882
Eracleous, M., & Halpern, J. P. 1994, ApJS, 90, 1
Esposito, P., Israel, G. L., Sidoli, L., et al. 2013, MNRAS, 433, 2028
Ghisellini, G., Tagliaferri, G., Foschini, L., et al. 2011, MNRAS, 411, 901
Grebenev, S. A., Lutovinov, A. A., Tsygankov, S. S., & Mereminskiy, I. A. 2013, MNRAS, 428, 50
Haberl, F., & Pietsch, W. 2004, A&A, 414, 667
Haberl, F., Eger, P., & Pietsch, W. 2008, A&A, 489, 327
Harries, T. J., Hilditch, R. W., & Howarth, I. D. 2003, MNRAS, 339, 157
Heckman, T. M. 1980, A&A, 87, 152
Ho, L. C., Filippenko, A. V., & Sargent, W. L. W. 1993, ApJ, 417, 63
Ho, L. C., Filippenko, A. V., & Sargent, W. L. W. 1997, ApJS, 112, 315
Ho, L. C., Rudnick, G., Rix, H.-W., et al. 2000, ApJ, 541, 120
Horne, K. 1986, PASP, 98, 609
Jones, D. H., Saunders, W., Colless, M., et al. 2004, MNRAS, 355, 747
Jones, D. H., Saunders, W., Read, M., & Colless, M. 2005, PASA, 22, 277
Kaspi, S., Smith, P. S., Netzer, H., et al. 2000, ApJ, 533, 631
Kauffmann, G., Heckman, T. M., Tremonti, C., et al. 2003, MNRAS, 346, 1055
Kaur, R., Wijnands, R., Paul, B., Patruno, A., & Degenaar, N. 2010, MNRAS, 402, 2388
Kennea, J. A. 2011, ATel #3578
Krivonos, R., Tsygankov, S., Sunyaev, R., et al. 2009, ATel #2170
Krivonos, R., Tsygankov, S., Revnivtsev, M., et al. 2010, A&A, 523, A61
Krivonos, R., Tsygankov, S., Lutovinov, A., et al. 2012, A&A, 545, A27
La Parola, V., Cusumano, G., Romano, P., et al. 2010, MNRAS, 405, L66
Landi, R., Masetti, N., Bassani, L., et al. 2007, ATel #1273
Landi, R., Masetti, N., Bazzano, A., et al. 2010, ATel #3065
Landi, R., Bassani, L., Masetti, N., et al. 2012a, ATel #4165
Landi, R., Bassani, L., Malizia, A., et al. 2012b, Swift/XRT observations of unidentified INTEGRAL/IBIS sources, in The Extreme and Variable High Energy Sky, Proc. of Science, pos.sissa.it, PoS(Extremesky 2011), 009
Landi, R., Bassani, L., Bazzano, A., Fiocchi, M., & Bird, A. J. 2013, Swift/XRT observations of newly discovered INTEGRAL sources, in An INTEGRAL view of the high-energy sky, the first 10 years, eds. A. Goldwurm, F. Lebrun, & C. Winkler, Proc. of Science, pos.sissa.it, PoS(INTEGRAL 2012), 098
Lang, K. R. 1992, Astrophysical Data: Planets and Stars (New York: Springer-Verlag)
Lanzuisi, G., De Rosa, A., Ghisellini, G., et al. 2012, MNRAS, 421, 390
Laurent-Muehleisen, S. A., Kollgaard, R. I., Ciardullo, R., et al. 1998, ApJS, 118, 127
Leicht, E. M., & Vasisht, G. 1998, New Astron., 3, 51
Luna, G. J. M., Sokoloski, J. L., Mukai, K., & Nuñez, N. 2012, ATel #3960
Lutovinov, A. A., Burenin, R. A., Revnivtsev, M. G., & Bikmaev, I. F. 2012, Astron. Lett., 38, 1
Maiorano, E., Landi, R., Parisi, P., et al. 2010, ATel #2975
Maiorano, E., Landi, R., Stephen, J. B., et al. 2011, MNRAS, 416, 531
Malizia, A., Stephen, J. B., Bassani, L., et al. 2009, MNRAS, 399, 944
Malizia, A., Bassani, L., Sguera, V., et al. 2010, MNRAS, 408, 975
Malizia, A., Landi, R., Bazzano, A., et al. 2011, ATel #3391
Malizia, A., Bassani, L., Landi, R., et al. 2012a, INTEGRAL view of the extragalactic sky, in: The Extreme and Variable High Energy Sky, Proc. of Science, pos.sissa.it, PoS(Extremesky 2011), 048
Malizia, A., Bassani, L., Bazzano, A., et al. 2012b, MNRAS, 426, 1750
Masetti, N., & Schiavone, F. 2008, IASF-Bologna Internal Report No. 522
Masetti, N., Palazzi, E., Bassani, L., Malizia, A., & Stephen, J. B. 2004, A&A, 426, L41 (Paper I)
Masetti, N., Mason, E., Bassani, L., et al. 2006a, A&A, 448, 547 (Paper II)
Masetti, N., Pretorius, M. L., Palazzi, E., et al. 2006b, A&A, 449, 1139 (Paper III)
Masetti, N., Bassani, L., Bazzano, A., et al. 2006c, A&A, 455, 11 (Paper IV)
Masetti, N., Morelli, L., Palazzi, E., et al. 2006d, A&A, 459, 21 (Paper V)
Masetti, N., Landi, R., Pretorius, M. L., et al. 2007, A&A, 470, 331
Masetti, N., Mason, E., Morelli, L., et al. 2008a, A&A, 482, 113 (Paper VI)
Masetti, N., Mason, E., Landi, R., et al. 2008b, A&A, 480, 715
Masetti, N., Parisi, P., Palazzi, E., et al. 2009, A&A, 495, 121 (Paper VII)
Masetti, N., Parisi, P., Palazzi, E., et al. 2010, A&A, 519, A96 (Paper VIII)
Masetti, N., Parisi, P., Jiménez-Bailón, E., et al. 2012a, A&A, 538, A123 (Paper IX)
Masetti, N., Jiménez-Bailón, E., Chavushyan, V., et al. 2012b, ATel #4248
Massey, P. 2002, ApJS, 141, 81
Mauch, T., Murphy, T., Buttery, H.J., et al. 2003, MNRAS, 342, 1117
Mescheryakov, A., Burenin, R., Sazonov, S., et al. 2009, ATel #2132
McDowell, J. C. 1994, Einstein Obs. Unscreened IPC Data Archive
McLure, R. J., & Jarvis, M. J. 2002, MNRAS, 337, 109
Minniti, D., Lucas, P.W., Emerson, J. P., et al. 2010, New Astron., 15, 433
Molina, M., Landi, R., Bazzano, A., et al. 2012a, ATel #4025
Molina, M., Landi, R., Bassani, L., et al. 2012b, A&A, 548, A32
Monet, D. G., Levine, S. E., Canzian, B., et al. 2003, AJ, 125, 984
Murphy, T., Mauch, T., Green, A., et al. 2007, MNRAS, 382, 382
Osterbrock, D. E. 1989, Astrophysics of Gaseous Nebulae and Active Galactic Nuclei (Mill Valley: Univ. Science Books)
Parisi, P., Masetti, N., Bassani, L., et al. 2012, ATel #4151
Paturel, G., Petit, C., Prugniel, P., et al. 2003, A&A, 412, 45
Predehl, P., & Schmitt, J. H. M. M. 1995, A&A, 293, 889
Pretorius, M. L. 2009, MNRAS, 395, 386

Ratti, E. M., van Grunsven, T. F. J., Torres, M. A. P., et al. 2013, MNRAS, 431, L10
Ricci, C., Bozzo, E., Walter, R., Paltani, S., & Stella, L. 2012, ATel #4345
Richards, G. T., Myers, A. D., Gray, A. G., et al. 2009, ApJS, 180, 67
Rieke, G. H., & Lebofsky, M. J. 1985, ApJ, 288, 618
Rodriguez, J. Tomsick, J. A., & Chaty, S. 2009, A&A, 494, 417
Rodriguez, J., Tomsick, J. A., & Bodaghee, A. 2010, A&A, 517, A14
Rojas, A., Masetti, N., & Minniti, D. 2012a, ATel #4006
Rojas, A., Masetti, N., & Minniti, D. 2012b, ATel #4342
Rojas, A., Masetti, N., & Minniti, D. 2013, ATel #4802
ROSAT Team 2000, ROSAT News No. 71
Saito, R. K., Hempel, M., Minniti, D., et al. 2012, A&A, 537, A107
Saxton R. D., Read, A. M., Esquej, P., et al. 2008, A&A, 480, 611
Scaringi, S., Bird, A. J., Norton, A. J., et al. 2010, MNRAS, 401, 2207
Schlegel, D. J., Finkbeiner, D. P., & Davis, M. 1998, ApJ, 500, 525
Sguera, V., Bazzano, A., Bird, A. J., et al. 2006, ApJ, 646, 452
Sguera, V., Hill, A. B., Bird, A. J., et al. 2007, A&A, 467, 249
Skrutskie, M. F., Cutri, R. M., Stiening, R., et al. 2006, AJ, 131, 1163
Smith, D. M., Markwardt, C. B., Swank, J. H., & Negueruela, I. 2012, MNRAS, 422, 2661
Stephen, J. B., Bassani, L., Malizia, A., et al. 2006, A&A, 445, 869
Strateva, I. V., Strauss, M. A., Hao, L., et al. 2003, AJ, 126, 1720
Sturm, R., Haberl, F., Pietsch, W., Immler, S., & Udalski, A. 2011, ATel #3575
Sturm, R., Haberl, F., Rau, A., et al. 2012, A&A, 542, A109
Sugizaki, M., Kinugasa, K., Matsuzaki, K., et al. 2000, PASJ, 52, 1141
Tomsick, J. A., Chaty, S., Rodriguez, J., Walter, R., & Kaaret, P. 2008, ApJ, 685, 1143
Tomsick, J. A., Bodaghee, A., Chaty, S., et al. 2012, ApJ, 754, 145
Townsend, L. J., Drave, S. P., Corbet, R. H. D., Coe, M. J., & Bird, A. J. 2011, ATel #3311
Townsend, L. J., Drave, S. P., Hill, A. B., et al. 2013, MNRAS, 433, 23
Trippe, M., Reynolds, C. S., Koss, M., Mushotzky, R. F., & Winter, L. M. 2011, ApJ, 736, 81
Ubertini, P., Lebrun, F., Di Cocco, G., et al. 2003, A&A, 411, L131
van Leeuwen, F. 2007, A&A, 474, 653
Veilleux, S., & Osterbrock, D. E. 1987, ApJS, 63, 295
Vestergaard, M. 2004, Black-Hole Mass Measurements, in AGN Physics with the Sloan Digital Sky Survey, eds. G. T. Richards, & P. B. Hall, ASP Conf. Ser., 311, 69 (San Francisco: ASP)
Voges, W., Aschenbach, B., Boller, T., et al. 1999, A&A, 349, 389
Voges, W., Aschenbach, B., Boller, T., et al. 2000, IAU Circ., 7432
Walter, R., Zurita Heras, J., Bassani, L., et al. 2006, A&A, 453, 133
Wang, Q., & Wu, X. 1992, ApJS, 78, 391
Warner, B. 1995, Cataclysmic variable stars (Cambridge: Cambridge University Press)
Watson, M. G., Schröder, A. C., Fyfe, D., et al. 2009, A&A, 493, 339
Wegner, W. 1994, MNRAS, 270, 229
Winkler, H. 1992, MNRAS, 257, 677
Winkler, C., Courvoisier, T.J.-L., Di Cocco, G., et al. 2003, A&A, 411, L1
Winter, L. M., Mushotzky, R. F., Tueller, J., & Markwardt C. B. 2008, ApJ, 674, 686
Wright, E. L. 2006, PASP, 118, 1711
Wu, X.-B., Wang, R., Kong, M. Z., Liu, F. K., & Han, J. L. 2004, A&A, 424, 793